Understanding totally asymmetric simple-exclusion-process transport on networks: Generic analysis via effective rates and explicit vertices

Ben Embley*
School of Chemical Engineering and Analytical Science, The University of Manchester, P.O. Box 88, Sackville Street, Manchester M60 1QD, United Kingdom

Andrea Parmeggiani†
Laboratoire de Dynamique des Interactions Membranaires Normales et Pathologiques, CNRS-UMR 5235, CC107, Université Montpellier II, Place Eugène Bataillon, 34095 Montpellier Cedex 5, France

Norbert Kern‡
Laboratoire des Colloïdes, Verres et Nanomatériaux, CNRS-UMR 5587, CC069, Université Montpellier II, Place Eugène Bataillon, 34095 Montpellier Cedex 5, France

(Received 15 April 2009; published 26 October 2009)

In this paper we rationalize relevant features of totally asymmetric simple-exclusion processes on topologies more complex than a single segment. We present a mean-field framework, exploiting the previously introduced notion of effective rates, which we express in terms of the average particle density on explicitly introduced junction sites. It allows us to construct the phase behavior as well as the current-density characteristic from well-known results for a linear totally asymmetric simple-exclusion-process segment in a very systematic and generic way. We validate the approach by studying a fourfold vertex in all variations in the number of entering/exiting segments and compare our predictions to simulation data. Generalizing the notion of particle–hole symmetry to take into account the topology at a junction shows that the average particle density at the junction constitutes a relevant directly observable parameter which gives detailed insight into the transport process. This is illustrated by a complete study of a simple network with figure-of-eight topology. Finally we generalize the approach to handle rate bias at a junction and discuss the surprisingly rich phenomenology of a biased figure-of-eight structure. This example highlights that the proposed framework is generic and readily extends to other topologies.

DOI: 10.1103/PhysRevE.80.041128 PACS number(s): 02.50.−r, 05.60.Cd

I. INTRODUCTION

One predominant model for one- and quasi-one-dimensional (quasi-1D) transports is undoubtedly the totally asymmetric simple-exclusion process (TASEP) [1,2]. It is conceptually simple but, being linked to real physical situations (cf. [3–6]), constitutes far more than a toy model. In TASEP, particles move in one direction along a segment of consecutive sites but are subject to the principle of excluded volume. This offers a simple model for the traffic of, for example, vehicles on roads [4,7,8] or motor proteins on biofilaments [9–11]. In this context, experimental work on biomimetic systems gives direct access to many aspects of such systems [12–14].

One of the many challenges facing the application of TASEP to real-world situations is the interconnectivity of a manifold of segments. Here we adopt the point of view, to our knowledge first presented in [15], that a useful way of analyzing quasi-1D transport on such a *network* is addressing it in terms of transport on many individual segments which meet at junction sites, at which coupling of the segmentwise transport arises. We shall show that this allows us to construct the overall phase behavior and transport characteristics of the combined system from known results for an individual segment and that the particle density measured locally at the junction site is a very useful directly measurable quantity for understanding transport on such networks.

Junctions have previously been introduced to TASEP models [15–17], and transport on a simple periodic hexagonal structure consisting of two threefold vertices per unit cell has been analyzed [18]. On the other hand, almost all networks occupying three-dimensional (3D) space require more complex topologies and in particular involve *fourfold* vertices. We may consider, for example, a Kelvin structure [19,20], which in some sense generalizes a hexagonal or "honeycomb" lattice to three dimensions. This regular structure, which arises naturally in foams, may be thought of as a bcc lattice of regular tetrakaidecahedrae (with slightly curved edges and faces) of the appropriate size [19]. In terms of the graph underlying this network topology, we deal with 12 fourfold vertices, but there is no obvious way of ascribing transport directions to the segments without further motivation from a concrete physical situation (e.g., particle advection in foam drainage under the effect of gravity: cf. [21]). We therefore focus on the behavior of a fourfold junction in all possible cases (one inlet and three outlets; two inlets and two outlets; and three inlets and one outlet) and characterize the associated transport properties in terms of "phase diagrams" for the stationary state. For brevity and clarity in the

*ben.embley@manchester.ac.uk
†andrea.parmeggiani@univ-montp2.fr
‡norbert.kern@univ-montp2.fr

following, we denote these vertices as V(1:3), V(2:2), and V(3:1), respectively: a vertex labeled as V(m:n) therefore represents a vertex with m incoming segments and n outgoing segments.

While all three cases may be relevant in 3D networks, a *symmetric* fourfold vertex V(2:2) is also representative of the crossing of quasi-1D segments *on a plane*, e.g., molecular motors [9] advancing on biofilaments confined to a surface which connect at contact points. In this connection, it could also be argued that a regular structure of such crossing points, forming a square lattice, is a yet simpler regular lattice than the honeycomb [18], albeit with a more complicated vertex, in terms of the number of its inlets and outlets. Consequently, we will also consider special cases of our analysis and link them to previous studies of crossing quasi-1D segments in different contexts [18,22,23].

Still in the spirit of generalizing the quasi-1D transport problem to 3D structures, beyond the question of a regular network, it is furthermore clear that in a real-world network of any realistic size we must expect *defects* and therefore *disorder* to interfere. Such disorder may intervene in many guises. We may distinguish *topological disorder* (for example, localized changes in connectivity in an otherwise regular network), *geometrical disorder* (differences in edge lengths), *directional disorder* (inverting transport directions in some segments), and *rate disorder* (e.g., segments with slower or faster particle hopping, biased distribution of particles onto outgoing segments of a junction, or reservoirs with modified rate constants). All these aspects concern disorder *inherent to the network* and therefore exceed the framework of local disorder that has previously been treated with respect to TASEP [24–32]. To this end, we will introduce generalizations to rate disorder in Sec. V, thereby preparing the analysis of more complex topologies.

The paper is organized as follows. In Sec. II we introduce a generic framework that allows us to analyze the mean-field [33] behavior of fourfold vertices in terms of the well-established behavior of individual TASEP segments with effective entrance/exit rates; we introduce the procedure on a well-understood example with trivial topology before extending it to the nontrivial problem of junctions. Section III applies this explicit-vertex framework to fourfold vertices of all three types, relates these fourfold vertices to special cases of studies previously mentioned [22,23], and compares theoretical and numerical (Monte Carlo) results. A simple network with a figure-of-eight topology is analyzed in Sec. IV. Finally, rate disorder, in the form of biased splitting at a junction site, is introduced in Sec. V. We conclude on the performance of the proposed explicit-vertex framework and discuss further perspectives in Sec. VI.

II. EXPLICIT-VERTEX FRAMEWORK

In this section we introduce what we call an *explicit-vertex method*. It is based on treating each segment as an open linear TASEP, for which the phase diagram is well known in terms of entrance/exit rates [34]. In principle, transport at a topological vertex might then be assumed to be governed by the net effect of overall effective rates, which essentially determine the overall frequency with which a particle entering through a given branch will exit through another given branch; this idea has been used in all the studies on junctions cited above. Here, however, our intention is to make these considerations applicable in a systematic way as to prepare the grounds for the study of networks of *arbitrary* topology. To this end we will show that it is useful to introduce the vertex *explicitly*, i.e., as an additional site: the particle density on the vertex will introduce a simple *linear* coupling between the entrance/exit rates for adjacent segments, thereby simplifying all calculations greatly. In this approach, the density at this junction site becomes the straightforward coupling parameter which ensures the matching between individual TASEP segments. Using only the condition of current conservation it then becomes straightforward to deduce the overall mean-field transport properties by combining the individual phase diagrams of all linear TASEP segments in a generic manner, as we shall now show.

A. Mean-field theory for a single TASEP segment: A brief reminder

Transport through a single TASEP segment has been studied by many authors in the past, and its main mechanisms are well understood. Current understanding includes many deep results in terms of exact solutions [35–43], fluctuations [24,41–47], as well as aspects of out-of-equilibrium thermodynamics [41–43,48–50] among others. Here we simply summarize the mean-field results in the form which we will exploit in the following sections of the paper; this serves to construct and introduce our approach to an analysis of transport on more complex structures.

Let us first recall that the average current J transported by a linear TASEP segments has the mean-field form,

$$J = \rho(1-\rho), \tag{1}$$

where ρ is the average particle density. The maximum current (MC) which can be achieved is $J_{\max}=1/4$, at half-filling $\rho=1/2$ (MC phase), where the subscript "max" will be used to identify maximum-current values. Any other given current may be sustained by either of the two different particle densities, which are generally denoted as the low-density (LD) and high-density (HD) solutions, according to the branch of the corresponding second-order equation [Eq. (1)].

The detailed mean-field diagram of a linear TASEP segment is best characterized [34] in terms of its entrance and exit rates, α and β, respectively. In the simplest case these rates are defined as the probability that a particle attempts to enter the first site of the segment from a reservoir (α) or that a particle leaves the segment from the last site (β), and both rates therefore take values in the domain $\alpha,\beta\in[0,1]$. Alternatively, these rates may be understood in terms of particle densities in the reservoirs, corresponding to a particle density of α in the reservoir supplying particles to the inlet, and a density of $1-\beta$ in the reservoir absorbing particles from the outlet. The possible combinations of α and β give rise to the three different phases already referred to as

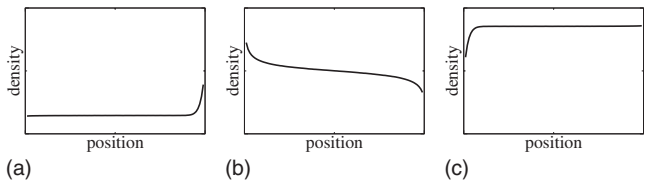

FIG. 1. Examples of the pure (a) LD, (b) MC, and (c) HD phases for TASEP. Particles are flowing from left to right, the boundary values for the density are α at the contact with the entrance reservoir and $1-\beta$ at the contact with the exit reservoir. Note that the curvatures of the LD and HD profiles may be convex or concave, depending on the actual values of the entrance/exit rates.

$$\begin{aligned} &\text{LD} \quad \text{if } \beta > \alpha \text{ and } \alpha < 1/2, \\ &\text{HD} \quad \text{if } \alpha > \beta \text{ and } \beta < 1/2, \\ &\text{MC} \quad \text{if } \alpha > 1/2 \text{ and } \beta > 1/2. \end{aligned}$$

The density profiles corresponding to these pure phases are reproduced in Fig. 1 for clarity and ease of reference.

The main physics in the bulk may be summarized by saying that the mean-field current given by Eq. (1) is accompanied by a bulk density ρ which is set by the *lower* of the two reservoir rates [34]; the behavior is thus dictated by the entrance rate if $\alpha<\beta$ and by the exit rate if $\beta<\alpha$. The exception arises for the MC phase: whenever *both* rates exceed 1/2, the current is sustained at its maximum level, maintaining the system at half-filling ($\rho=1/2$). We shall refer to these three cases as "phases," as is commonly done.

This picture is of course incomplete, since the density cannot extend throughout the segment at its bulk value, but must develop boundary zones in order to adapt to the particle exchange at the edges of a segment or, said another way, in order to match the reservoir densities at its boundaries. This matching is in fact so crucial that the term of *boundary-induced phase transitions* has been coined [51]. Bypassing all subtleties, the values for the density at the boundaries of the segment (i.e., the first and the last sites) may be inferred directly from current conservation, again in a mean-field spirit. For example, the entrance density $\rho_{(\mathrm{HD})}^{(\mathrm{IN})}$ at the first site of HD segment must respect the condition

$$\alpha(1-\rho_{\mathrm{HD}}^{(\mathrm{IN})}) = J_{\mathrm{HD}} = \beta(1-\beta) \tag{2}$$

since the current at any position may be obtained as the rate at which a particle move is attempted and the probability for it to succeed. Thus,

$$\rho_{\mathrm{HD}}^{(\mathrm{IN})} = 1-\beta\frac{(1-\beta)}{\alpha}. \tag{3}$$

The relevant bulk and boundary values for the density are given in Table I for all such phases. It is at this level of mean-field description that we pursue our analysis, neglecting the many more subtle details which are known about the physics of the associated boundary layers [52].

B. Test case: Coupling two TASEP segments in series

The simplest possible case we can consider is two consecutive linear TASEP segments linked through a "junction" site. We discuss this example in some detail even though applying the approach to this trivial example may appear overly complicated and can only lead to the obvious behavior; this not only serves as a test case but also as a "tutorial example": going through all the conceptual steps in this simple case allows us to illustrate the procedure and pave the way for analyzing more complex topologies.

TABLE I. Mean-field expressions for currents and bulk as well as boundary densities for a single TASEP segment with entrance rate α and exit rate β.

Phase	Current	Bulk density	Entrance/exit densities	
LD	$J_{\mathrm{LD}}=\alpha(1-\alpha)$	$\rho_{\mathrm{LD}}=\alpha$	$\rho_{\mathrm{LD}}^{(\mathrm{IN})}=\alpha$	$\rho_{\mathrm{LD}}^{(\mathrm{OUT})}=\alpha\frac{(1-\alpha)}{\beta}$
HD	$J_{\mathrm{HD}}=\beta(1-\beta)$	$\rho_{\mathrm{HD}}=1-\beta$	$\rho_{\mathrm{HD}}^{(\mathrm{IN})}=1-\beta\frac{(1-\beta)}{\alpha}$	$\rho_{\mathrm{HD}}^{(\mathrm{OUT})}=1-\beta$
MC	$J_{\mathrm{MC}}=\frac{1}{4}$	$\rho_{\mathrm{MC}}=\frac{1}{2}$	$\rho_{\mathrm{MC}}^{(\mathrm{IN})}=\frac{1}{4\alpha}$	$\rho_{\mathrm{MC}}^{(\mathrm{OUT})}=\frac{1}{4\beta}$

Consider thus two segments, A and B, the former receiving particles from a reservoir at density α (entrance rate α), whereas the latter disposes of particles into a reservoir at density $1-\beta$ (exit rate β). The physical question we are asking is the following: for a given set of (overall) entrance/exit rates (α,β), what is the current flowing through the system and what phases do we expect to see?

1. Junction site and effective rates

Let us therefore introduce an additional junction site, identified by a tilde—which in this simple case is in fact just another regular site—at which the individual segments (A and B, say) connect (cf. Fig. 2). The mean-field currents entering/exiting each segment are given as follows:

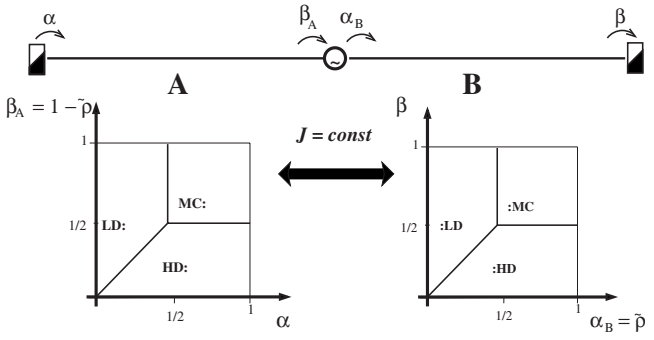

FIG. 2. Schematic of a (trivial) twofold vertex V(1:1), i.e., two successive linear TASEP segments coupled via a junction site (labeled as $\tilde{}$). α and β are the overall entrance and exit rates, respectively. β_{A} and α_{B} are the effective exit/entrance rates at the points where the segments connect to the junction. The phase diagram of each segment is that of linear TASEP, where the abscissa is the effective entrance rate to a segment, while the ordinate is the effective exit rate from the same segment. The coupling is implemented by expressing the effective rates which link "segments" to the junction site in terms of that site's density $\tilde{\rho}$. Current conservation then supplies the matching condition required to determine the phases of the combined system. Although a vertex V(1:1) is trivial, the example serves to illustrate our approach. Phases of the subsystems are labeled HD: for a high-density phase of the incoming segment and :LD for a low-density phase of the outgoing segment, etc.

$$\text{segment A: } J_A^{(\mathrm{IN})} = \alpha(1-\rho_A^{(\mathrm{IN})}), \quad J_A^{(\mathrm{OUT})} = \rho_A^{(\mathrm{OUT})}(1-\tilde{\rho}),$$

$$\text{segment B: } J_B^{(\mathrm{IN})} = \tilde{\rho}(1-\rho_B^{(\mathrm{IN})}), \quad J_B^{(\mathrm{OUT})} = \rho_B^{(\mathrm{OUT})}(1-\beta). \tag{4}$$

Within a mean-field interpretation this is identical to describing the situation *as if* the junction site was a reservoir of density $\tilde{\rho}$, to which both segments are coupled. This evidently sets the *effective rates*, at which particles enter/exit the adjacent individual segments. In the following such effective entrance/exit rates for a given segment will be identified through a subscript indicating the concerned segment, whereas we reserve the rates α, β without subscript for a boundary condition given as an overall entrance/exit rate, i.e., generally set by coupling to an external reservoir,

$$\text{segment A: } \alpha_A = \alpha, \quad \beta_A = 1-\tilde{\rho},$$

$$\text{segment B: } \alpha_B = \tilde{\rho}, \quad \beta_B = \beta. \tag{5}$$

They furthermore satisfy the relation

$$\beta_A = 1-\alpha_B, \tag{6}$$

which therefore characterizes the (in this case trivial) topological coupling between the two segments at the junction.

One remark of caution is in order: the proposed approach retains the average particle density on the junction site as sole parameter for describing the behavior of this site. This reflects the mean-field spirit of the analysis, and consequently correlation effects cannot be expected to be captured correctly. We shall argue below that this limitation implies subtleties when coexisting phases arise.

The choice of retaining an explicit site at the junction may seem artificial compared to defining a (different) effective rate for crossing over directly from one segment to the next in one step, as has been done before, explicitly or implicitly [16,17,26]. Several remarks are in order. First, it is clearly useful to express both effective rates in terms of a physical, measurable parameter, the particle density at the junction site ($0 \le \tilde{\rho} \le 1$); we will examine predictions for $\tilde{\rho}$ later. Second, any effective rate for direct crossing is in fact a product of two probabilities, one for attempting to leave one segment and another one for being accepted onto the next. Using the junction density $\tilde{\rho}$, on the other hand, decouples these two steps: this will be a crucial feature for constructing the overall phase behavior in the presence of branching.

2. Segmentwise currents

To find the current and the phases we may now argue as follows. The overall entrance/exit rates, α and β, are the physical parameters which are imposed. Given their values, the density $\tilde{\rho}$ at the junction is the degree of freedom which must adjust in order to match the two mean-field solutions; the matching criterion is the *continuity of the current at the junction site* (cf. Fig. 2). We may deduce the current through segment A at given entrance/exit rates α and β_A from the standard mean-field results for TASEP recalled above (cf. Table I). The analogous result applies to segment B.

Expressing currents as a function of the junction density and using the effective rates defined above we have, for segment B,

$$J_B(\tilde{\rho};\beta) = \begin{cases} \tilde{\rho}(1-\tilde{\rho}) & \text{if } \tilde{\rho} < \beta, \quad \tilde{\rho} < 1/2 \quad (\mathrm{B=LD}) \\ \beta(1-\beta) & \text{if } \tilde{\rho} > \beta, \quad \beta < 1/2 \quad (\mathrm{B=HD}) \\ 1/4 & \text{if } \tilde{\rho}, \quad \beta > 1/2 \quad (\mathrm{B=MC}). \end{cases} \tag{7}$$

In order not to overload the notation we have not specified the behavior on the phase boundaries here, but we point out that a B=LD/HD coexistence on segment B arises [36] whenever the effective entrance rates of this segment are equal and inferior to 1/2, i.e., whenever $\tilde{\rho}=\beta<1/2$: we shall return to this point later. Similarly, the current through segment A at given exit rate β is, using Eq. (5),

$$J_A(\alpha;\tilde{\rho}) = \begin{cases} \alpha(1-\alpha) & \text{if } \tilde{\rho} < 1-\alpha, \quad \alpha < 1/2 \quad (\mathrm{A=LD}) \\ \tilde{\rho}(1-\tilde{\rho}) & \text{if } \tilde{\rho} < 1-\alpha, \quad \tilde{\rho} > 1/2 \quad (\mathrm{A=HD}) \\ 1/4 & \text{if } \alpha > 1/2, \quad \tilde{\rho} < 1/2 \quad (\mathrm{A=MC}). \end{cases} \tag{8}$$

A LD/HD coexistence on segment A arises whenever $1-\tilde{\rho}=\alpha<1/2$.

3. Current matching at the junction

These two mean-field expressions for the segmentwise currents must be matched (cf. illustration in Fig. 2). We may thus proceed for any given pair of rates (α,β) by plotting $J_A(\alpha;\tilde{\rho})$ and $J_B(\tilde{\rho};\beta)$ as a function of $\tilde{\rho}$ and finding the intersection of the two curves, such that $J_A(\alpha;\tilde{\rho})=J_B(\tilde{\rho};\beta)$. These functions are defined piecewise, according to the phase of the corresponding segment: Fig. 3 represents schematically an example for this operation. Furthermore, since $J_A(\alpha;\tilde{\rho})$ decreases monotonically *to* zero (for $\tilde{\rho}=1$) whereas $J_B(\tilde{\rho};\beta)$ increases monotonically *from* zero (for $\tilde{\rho}=0$), we are guaranteed that there exists a physical solution and that it is unique.

4. Phases of the combined system

Carrying out this procedure for the entire parameter space (α,β) we find the overall system in coinciding phases (LD:LD, HD:HD, or MC:MC) but also a mixed phase (HD/MC):(LD/MC), where we use the symbol "/" to indicate that the corresponding segment is in fact in a state on the phase boundary between the two given phases. The coinciding phases are intuitively expected (the combined system behaves just as one long segment), but the mixed state may come as some surprise. At first sight this seems to suggest that the upstream segment A is in a HD state, whereas the downstream segment B is in a LD state, amounting to a HD-LD domain wall in the combined system. The latter is, however, known to be unstable on a linear TASEP segment [47]. This apparent contradiction is resolved through the interplay of entrance/exit densities of the individual segments. To see this, we note that the density profile of segment A on the HD/MC phase boundary is characterized, using Table I, by

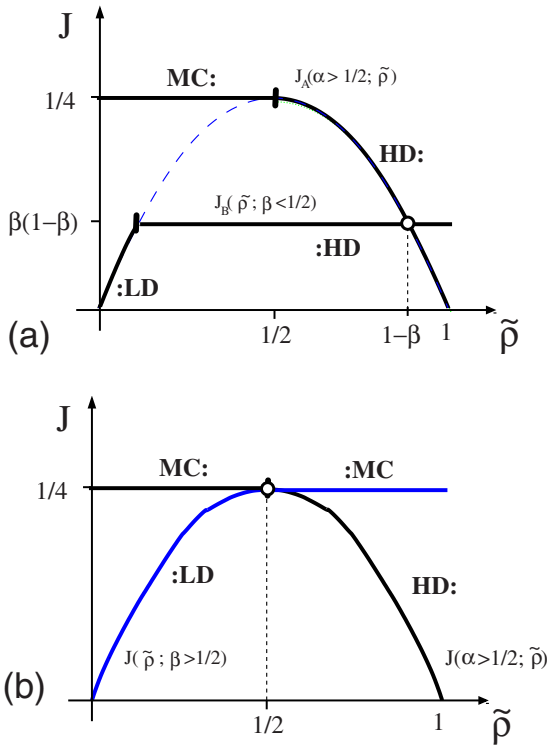

FIG. 3. (Color online) Examples of the current-matching procedure (cf. Sec. II B) at a junction for the trivial case V(1:1). For this schematic, we plot $J_A(\alpha;\tilde{\rho})$ and $J_B(\tilde{\rho};\beta)$, the intersection of which (labeled by a circle) corresponds to the physical solution for which the currents match correctly. Segments of the individual curves are labeled to indicate the phase they correspond to, and the nature of the physical solution may therefore be determined by reading off the phases of each segment at the point of intersection. The corresponding density at the junction $\tilde{\rho}$ may also be read off directly. In (a), $\alpha \geq 1/2$ and $\beta < 1/2$; in (b), $\beta > \alpha > 1/2$. The sequence (a) to (b) shown therefore illustrates the switching of the solution as the exit rate $\beta = 0, \ldots, 1$ sweeps out its entire range and $\alpha > 1/2$ is kept constant. Here we switch from a HD:HD solution [i.e., in (a)] to the rather particular case where the overall solution, MC/HD:MC/LD, involves coexisting phases in both of segments A and B [i.e., in (b)]. This latter case corresponds a junction density of $\tilde{\rho} = 1/2$.

$$\rho_{\mathrm{A=HD/MC}} = \frac{1}{2}, \quad \rho^{(\mathrm{IN})}_{\mathrm{A=HD/MC}} = 1 - \frac{1}{4\alpha}, \quad \rho^{(\mathrm{OUT})}_{\mathrm{A=HD/MC}} = \frac{1}{2}, \tag{9}$$

whereas the density of segment B on the LD/MC evaluates to

$$\rho_{\mathrm{B=HD/MC}} = \frac{1}{2}, \quad \rho^{(\mathrm{IN})}_{\mathrm{B=HD/MC}} = \frac{1}{2}, \quad \rho^{(\mathrm{OUT})}_{\mathrm{B=HD/MC}} = 1 - \frac{1}{4\beta}. \tag{10}$$

Note also that the density at the junction is found to be $\tilde{\rho} = 1/2$ in this case, as illustrated by the second example given in Fig. 3. The mixed phase therefore corresponds in reality to the two segments being joined seamlessly at the junction through a flat profile at bulk density 1/2, with the boundary densities of the combined system A:B being given as

$$\rho_{\mathrm{A:B}} = \frac{1}{2}, \quad \rho^{(\mathrm{IN})}_{\mathrm{A:B}} = 1 - \frac{1}{4\alpha}, \quad \rho^{(\mathrm{OUT})}_{\mathrm{A:B}} = 1 - \frac{1}{4\beta}, \tag{11}$$

that is, values which correspond precisely to what is expected for one large segment in the MC phase [cf. Fig. 1(b) for a schematic and Table I for exact boundary values].

In conclusion for this simple example, we have combined two TASEP segments into a (single) large one, coupling them through an intermediate junction site, the density of which is the degree of freedom allowing us to match the segment currents. The argument is straightforward and generic and leads to consistent results at the mean-field level, provided only that we distinguish entrance/exit densities of each segment from their mean-field bulk density.

C. Branching

Beyond this test case, which has served to introduce and illustrate the spirit of our analysis, it is now obvious that the coupling through a junction site generalizes to nontrivial junctions. Consider a junction linking m incoming segments $\mathrm{A}_1, \ldots, \mathrm{A}_m$ to n outgoing ones $\mathrm{B}_1, \ldots, \mathrm{B}_n$. We may define effective rates for this vertex of form V(m:n) exactly as above,

$$\beta_{\mathrm{A}} := \beta_{\mathrm{A}_1} = \cdots = \beta_{\mathrm{A}_m} = 1 - \tilde{\rho},$$

$$\alpha_{\mathrm{B}} := \alpha_{\mathrm{B}_1} = \cdots = \alpha_{\mathrm{B}_n} = \frac{1}{n} \times \tilde{\rho}, \tag{12}$$

where throughout we use the notation $n\times$ in order to emphasize prefactors which are directly related to the topological aspects of the system.

The observations made above therefore generalize to a more complex network: for each junction joining several linear segments, we may introduce an additional junction site. The average number of particles carried by this junction ($\tilde{\rho}$) is the degree of freedom which must be adjusted to match the currents through it. We therefore establish one additional condition for each additional degree of freedom associated to a junction, and this constraint takes the particularly simple form of a *linear* relation between the effective rates coupling the adjacent segments to the junction site.

Before proceeding to analyze the case of a *fourfold vertex* in detail, it will be useful to outline the notation we shall use to represent branched structures. As above, we use the colon to denote a succession of substructures (e.g., A:B:…:Z). Any of these may in the simplest case be linear TASEP segments, as in the example above, or a more complicated arrangement of segments and junctions. Similarly, we use the "‖" symbol to indicate "parallel" branches (e.g., A‖B‖…‖Z). Parentheses are then required to express precedence in order to unambiguously identify the underlying topology, e.g., to distinguish the most general case of a V(2:2) fourfold vertex :(A‖B):(C‖D): from three parallel segments, the middle one of which is composed of two independent segments :A‖(B:C)‖D: [see Fig. 4(b) for an illustration]. In

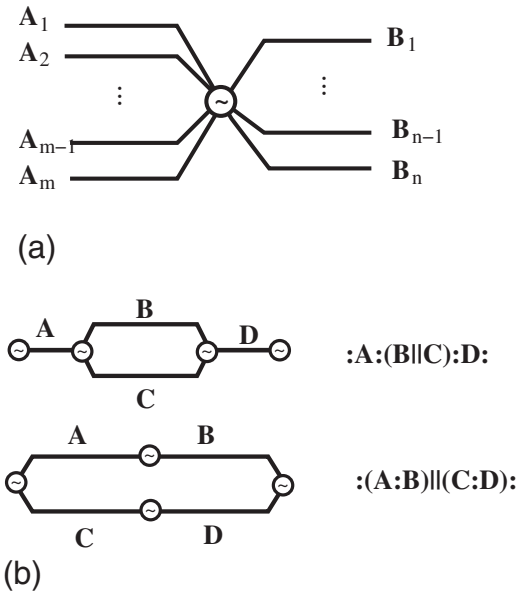

FIG. 4. (a) Schematic of a V(m:n) junction, i.e., a junction with m incoming segments and n outgoing segment. The junction is labeled with a tilde. (b) Illustration for notation of topologies.

the context of networks, it is convenient to give precedence to the connector ‖ over the connector ":" since dividing a segment into subsegments is only useful in particular cases, such as the presence of point defects.

III. FOURFOLD VERTEX

In turn, we will analyze the three relevant variants of a fourfold vertex (excluding pathological cases for which there are no entering or no exiting segments), maintaining for the time being the restriction that the same input rate α be applied to all incoming vertices and that the same output rate β be applied to all outgoing segments.

A. Two in, two out—V(2:2)

The vertex V(2:2), with two incoming and two outgoing branches, is schematically represented in Fig. 5.

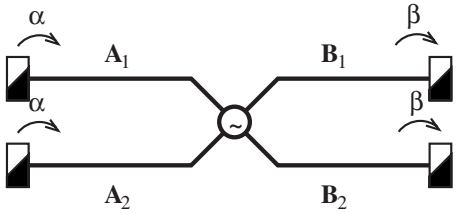

FIG. 5. Schematic representation of the fourfold junction V(2:2) as used for the explicit-vertex analysis. Both incoming branches couple to a reservoir at density α and both outgoing segments couple to a reservoir at density $1-\beta$. Phases are labeled as "2A:2B," e.g., 2HD:2LD stands for both incoming segments in a high-density phase ($A_1=A_2=$HD) and both outgoing segments in a low-density phase ($B_1=B_2=$LD). Note that we have simplified the notation based on symmetry, writing 2A:2B rather than "$(A_1\|A_2):(B_1\|B_2)$."

1. Effective rates and mapping onto linear TASEP

As discussed above, we may assign effective rates to each of the segments linking to the vertex; these are

$$\mathrm{A}_{1,2}:\ \alpha_{\mathrm{A}_{1,2}}=\alpha,\quad \beta_{\mathrm{A}_{1,2}}=1-\tilde{\rho},$$

$$\mathrm{B}_{1,2}:\ \alpha_{\mathrm{B}_{1,2}}=\tilde{\rho}/2,\quad \beta_{\mathrm{B}_{1,2}}=\beta. \tag{13}$$

In a mean-field approach branches A_1 and A_2 obviously behave identically, from symmetry, and so do branches B_1 and B_2, which we express by noting $\alpha_{\mathrm{A}_{1,2}}=\alpha_{\mathrm{A}_1}=\alpha_{\mathrm{A}_2}$ and similarly for branches B.

In terms of the standard TASEP phase diagram [34], the relation $\alpha_{\mathrm{B}_{1,2}}=\tilde{\rho}/2$ captures the fact that segments B_1 and B_2 share their input site (the junction). Since particles can only move into either of the branches, this is reflected in the effective entrance rate of the following segments, which therefore remains reduced: $\alpha_{\mathrm{B}_{1,2}}\leq 1/2$ (since $\tilde{\rho}\leq 1$). As a consequence, in terms of the TASEP phase behavior in the outgoing segments B_1, B_2, only some of the (otherwise possible) phases are accessible. In particular, a maximum-current phase cannot arise in the outgoing branches.

In Fig. 6, we present the resulting TASEP-like phase diagrams for the incoming and the outgoing branches. Rather than using the entrance/exit rates as variables, as is commonly done for linear segments, we label the axes in terms of the junction density $\tilde{\rho}$ where this is applicable: this has the advantage of constructing the argument using a physical degree of freedom, facilitates the construction of the combined phase diagram, and, since $\tilde{\rho}\in[0,1]$, correctly incorporates the fact that the effective rates [cf. Eq. (13)] are restricted to certain intervals.

2. Current matching

To this end we proceed as in the example above, i.e., we fix the reservoir rates (α,β) and solve for the junction density $\tilde{\rho}$ by matching the currents through the segments,

$$J_{\mathrm{A}_1}=J_{\mathrm{A}_2}=J_{\mathrm{B}_1}=J_{\mathrm{B}_2}, \tag{14}$$

where we have again exploited the equivalence between branches.

It is now useful to structure the analysis in terms of cases for the input/output rates. As an example consider the case $\alpha,\beta>1/2$ to further illustrate the procedure. Figure 7 shows a sketch of the currents as a function of $\tilde{\rho}$ for $\alpha,\beta>1/2$, where

$$J_{\mathrm{A}_{1,2}}\left(\alpha>\tfrac{1}{2};\tilde{\rho}\right)=\begin{cases}\tilde{\rho}(1-\tilde{\rho}) & \text{if } \tilde{\rho}>\tfrac{1}{2}\ (\text{'HD:'}\ \text{phase})\\ \tfrac{1}{4} & \text{if } \tilde{\rho}<\tfrac{1}{2}\ (\text{'MC:'}\ \text{phase}),\end{cases} \tag{15}$$

whereas

$$J_{\mathrm{B}_{1,2}}\left(\tilde{\rho};\beta>\tfrac{1}{2}\right)=\frac{\tilde{\rho}}{2}\left(1-\frac{\tilde{\rho}}{2}\right), \tag{16}$$

since the outlets are necessarily in a ":LD" phase. The currents through the branches are therefore compatible for the

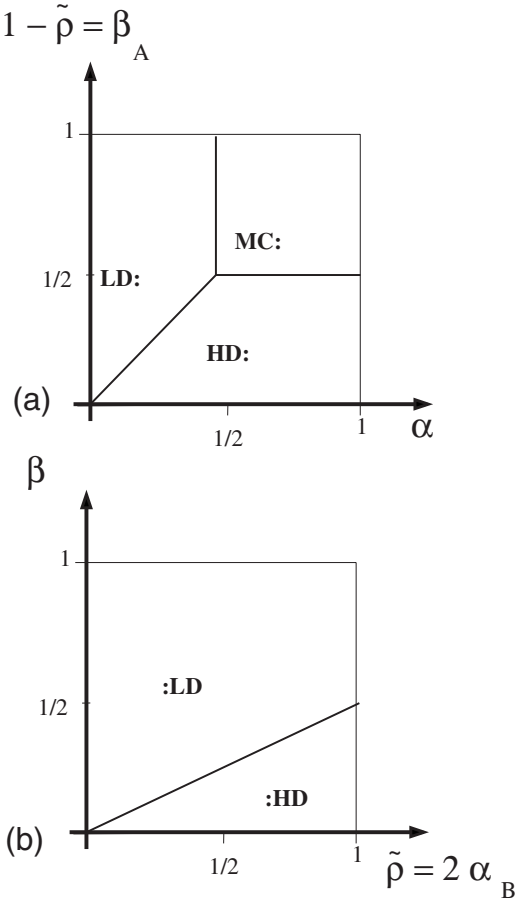

FIG. 6. Mean-field phases for the individual segments of V(2:2): (a) incoming segments (A_1,A_2), identical to linear TASEP, and (b) for outgoing segments (B_1,B_2), with a rescaled axis such that only part of the linear TASEP behavior is accessible. The effective rates linking segments to the junction site are expressed in terms of the junction density $\tilde{\rho}$, which subsequently makes it easier to deduce the phase behavior of the overall system. In order to distinguish incoming and outgoing segments, we label the subsystems HD: for a high-density phase of an incoming segment, :LD for a low-density phase of an outgoing segments, etc.

particular junction density $\tilde{\rho}^*=2/3$, and the solution evaluates as $J_A^*=J_B^*=2/9$ whatever the actual values within the domain $\alpha,\beta>1/2$. The resulting combined phase is "2HD:2LD" since it is between these branches of the current characteristics $J(\tilde{\rho})$ that current matching is achieved.

3. Phase behavior

Proceeding to all other cases and following the same line of argument, we predict the phase diagram for a vertex of type V(2:2), as is shown in Fig. 8. It is rather similar to that of a linear TASEP segment in that the lower of the rates (α,β) determines the transport, imposing a low density on all segments if transport is entrance-limited $(\alpha<\beta)$ or a high density on all segments if transport is exit- limited $(\beta<\alpha)$. This example furthermore features a *saturated current* whenever $\alpha,\beta>1/3$. This phase too may be interpreted in the same spirit as a MC phase on a simple linear segment in that the current has achieved a maximum value, which no longer

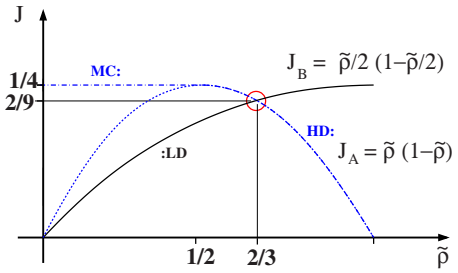

FIG. 7. (Color online) Illustration of the current-matching procedure for one particular case $(\alpha,\beta>1/2)$ of V(2:2). The current through any individual segment is known in terms of its input/output rates, which are $(\alpha,1-\tilde{\rho})$ and $(\tilde{\rho}/2,\beta)$, respectively. For a given pair (α,β), the currents $J_{A_{1,2}}(\alpha;\tilde{\rho})$ and $J_{B_{1,2}}(\tilde{\rho};\beta)$ are piecewise functions of $\tilde{\rho}$ [illustrated here for the domain $\alpha,\beta>1/2$; cf. Eqs. (15) and (16)]. The current flowing through the segments are compatible at the intersection of the two curves, which fixes the junction density (here $\tilde{\rho}=2/3$, irrespective of α and β) and therefore the current $J=2\times J_{A_1,A_2}=2\times J_{B_1,B_2}=2\times 2/9$ crossing the system. The corresponding phases are determined from the parts of the current relations at which the intersection occurs (here A_1,A_2 =HD: and B_1,B_2=:LD). Once the input as well as the output rates exceed 1/2, the system is therefore in a state where the current saturates at a value of $J_{\max}=2\times 2/9$, irrespective of the actual values of these rates.

varies in terms of the rates α and β whenever *both* rates exceed a certain threshold. Here, however, this threshold is lowered to 1/3 (compared to 1/2 in the linear segment) and, rather than a MC phase, we observe a phase of type 2HD:2LD, such that particles are concentrated in the upstream segments where they pile up before entering the junction. The particle current achieved in this saturated phase is

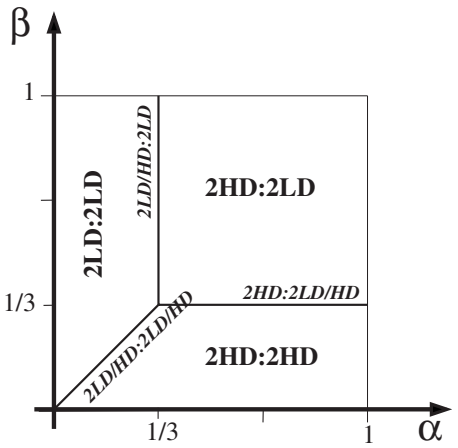

FIG. 8. Mean-field phase diagram for a fourfold junction V(2:2), where both incoming branches couple to a reservoir at density α and both outgoing segments couple to a reservoir at density $1-\beta$. Phases are labeled as "$A_{1,2}$:$B_{1,2}$," e.g., 2HD:2LD stands for both incoming segments in a high-density phase ($A_{1,2}$=$B_{1,2}$=HD) and both outgoing segments in a low-density phase ($A_{1,2}$=$B_{1,2}$=LD). The labels along the transition lines recall that these correspond to coexisting phases in the *individual* segments: for example, the phase boundary line on $\beta=1/3$ involves segment A being in a HD phase, whereas a LD/HD coexistence is induced on segment B.

lower than what would correspond to two independent parallel linear TASEP segments, $J_{\max}=2\times\rho(1-\rho)=2\times\frac{2}{9}$, which is smaller than $2\times\frac{1}{4}$, but the difference is rather small, hinting at the fact that the hindrance through the shared junction site is not as important as one might have expected intuitively; we shall return to this point later (cf. Sec. IV). Furthermore, we already mention another major novelty with respect to the MC phase in linear TASEP for the transport characteristic expressed through the functional form of $J(\rho)$ for closed or periodic-on-average systems: whereas the MC current in linear TASEP corresponds to a particular value of the density ($\rho=1/2$), the saturated current in V(2:2) is achieved for an entire *range* of densities, thus giving rise to a plateau in the transport characteristic. We shall link this to the occurrence of domain walls in a later section (cf. Sec. V).

4. Overall current

Further information is obtained from the current $J(\alpha,\beta)$ associated with these phases, defined as the current passing through the system (and therefore identical to the current passing the junction site but *twice* the current passing through any individual segment). It reads

$$J(\alpha,\beta) = \begin{cases} 2\times\alpha(1-\alpha) & \text{2LD:2LD}, \quad \text{i.e.,} \quad \alpha<\frac{1}{3}, \quad \beta>\alpha \\ 2\times\frac{2}{9} & \text{2HD:2LD}, \quad \text{i.e.,} \quad \alpha, \quad \beta>\frac{1}{3} \\ 2\times\beta(1-\beta) & \text{2HD:2HD}, \quad \text{i.e.,} \quad \beta<\frac{1}{3}, \quad \alpha>\beta. \end{cases} \tag{17}$$

We also state the corresponding density at the junction site, as obtained in the same analysis, for future reference,

$$\tilde{\rho}(\alpha,\beta) = \begin{cases} 2\alpha & \text{2LD:2LD}, \quad \text{i.e.,} \quad \alpha<\frac{1}{3}, \quad \beta>\alpha \\ \frac{2}{3} & \text{2HD:2LD}, \quad \text{i.e.,} \quad \alpha, \quad \beta>\frac{1}{3} \\ 1-\beta & \text{2HD:2HD}, \quad \text{i.e.,} \quad \beta<\frac{1}{3}, \quad \alpha>\beta. \end{cases} \tag{18}$$

Consequently, for the V(2:2), the current is a continuous function of the parameters (α,β), but a discontinuity in its derivative is associated with all phase boundaries. In particular, the transitions toward the saturated 2HD:2LD phase may therefore be termed "discontinuous," which constitutes another difference with respect to a MC phase on a linear segment.

5. Numerical confirmation

In order to verify our results independently and to critically judge the validity of the mean-field approach, we have performed extensive numerical simulations in which each branch consists of $L=100$ sites. In the Monte Carlo process, we randomly select a site and, whenever it contains a particle and its downstream nearest neighbor is vacant, we move the particle forward to the next site. From the junction site, branches B_1 and B_2 are selected with equal probability. Particle insertion from a reservoir into the entrance of the segment is attempted with rate α, whereas particles on the exit site are absorbed into another reservoir with probability β. Our time unit is one "cycle," defined as the time period in which each site is, on average, selected once. Upon initialization, the system is allowed to relax for 10^6 cycles before any measurements are performed. We then measure the total current J, the overall density ρ, and the density $\tilde{\rho}$ on the junction for many sets of reservoir rate parameters (α,β). Figure 9 shows both the measured current as a function of (α,β) and a two-dimensional (2D) projection of the same data in terms of reservoir rates in order to probe the predictions for transition lines. In both cases, the data symbols correspond to the phases observed in simulation, whereas the solid lines indicate mean-field predictions for the transition

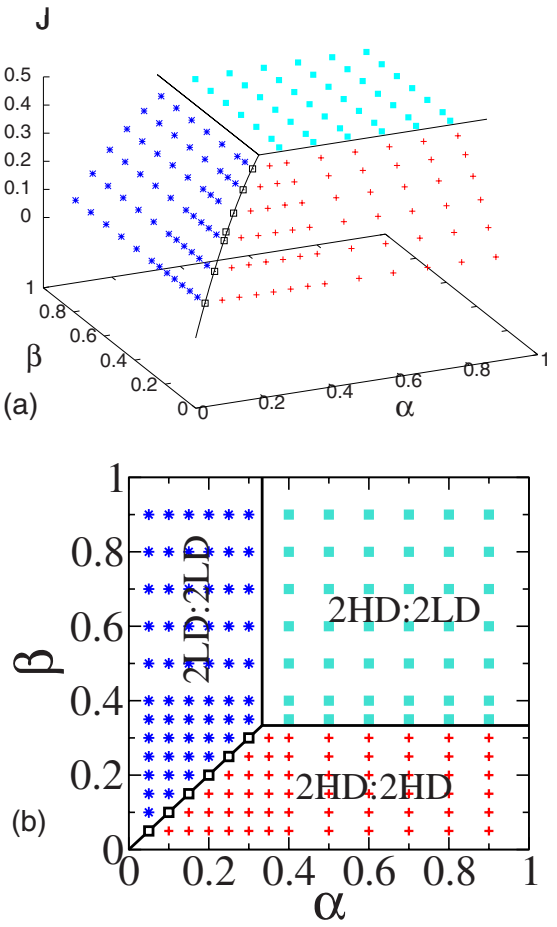

FIG. 9. (Color online) Current flowing through a fourfold vertex V(2:2). The current is continuous, but, at all phase boundaries, its slope is not. In (a), we plot the (simulation) total current J as a function of both α and β; a two-dimensional projection is shown in (b). We examine all cases of (α,β) and plot (as a minimum) a 10×10 grid of points (α,β), with extra points close to certain transition lines. We also detect the phase combination directly from simulation, which are represented through the data symbols: data detected as 2LD:2LD are plotted as (blue) stars, 2HD:2LD as (turquoise) squares, and 2HD:2HD as (red) crosses; black squares (unfilled) are data for which either LD or HD phases are detected in each branch (i.e., 2LD/HD:2LD/HD coexistence: cf. Fig. 8 and also [18] for a method of domain wall detection). The black lines represent *theoretical* phase boundaries, based on Eq. (17), which are thus corroborated by the simulation data.

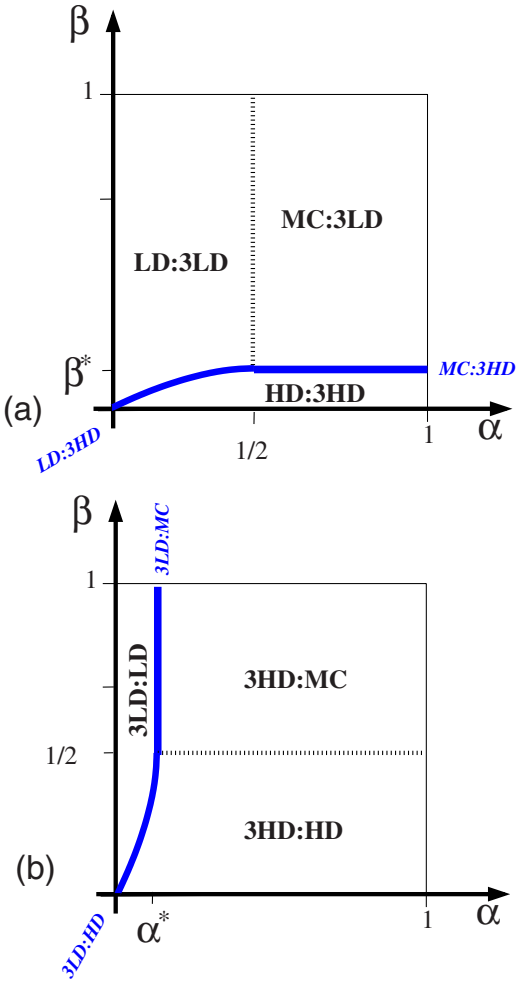

FIG. 10. (Color online) Mean-field phase diagram for (a) a fourfold junction V(1:3) where the incoming branch is coupled to a reservoir at density α and all three outgoing segments coupled to a reservoir at density $1-\beta$, as obtained by an effective-rate analysis similar to the one for the symmetric case V(2:2) (cf. Sec. III B). The value indicated on the β axis, which characterizes the boundary between HD:3HD and MC:3LD, is $\beta^*=\frac{1}{2}-\frac{1}{\sqrt{6}}\approx 0.09$. The separation line between phases HD:3HD and LD:3LD obeys $\alpha(1-\alpha)=3\times\beta(1-\beta)$. (b) In this phase diagram for a junction V(3:1) (cf. Sec. III C), the value indicated on the α axis is $\alpha^*\approx 0.09$, i.e., the same as β^* in the previous figure. The separation line between phases 3LD:LD and 3HD:HD obeys $3\times\alpha(1-\alpha)=\beta(1-\beta)$. Labels in italics refer to the phase boundaries *only*; dotted phase boundaries indicate continuous transitions.

lines. The resulting diagram shows good agreement between Eq. (17) and the Monte Carlo simulations: for $\alpha,\beta>1/3$ a saturated-current phase (cf. Fig. 7) is obtained; meanwhile, if one or more of the reservoir rates $\alpha,\beta<1/3$, the lower value takes on the role of a *limiting rate*.

6. Critical values at the phase boundaries

To complete our discussion we now explain the critical rate values $\alpha^*=\beta^*=1/3$, which characterize the phase boundaries. To this end, let us fix $\beta>1/3$ and $\alpha<1/3$ and observe what happens as α is increased. Since the system is

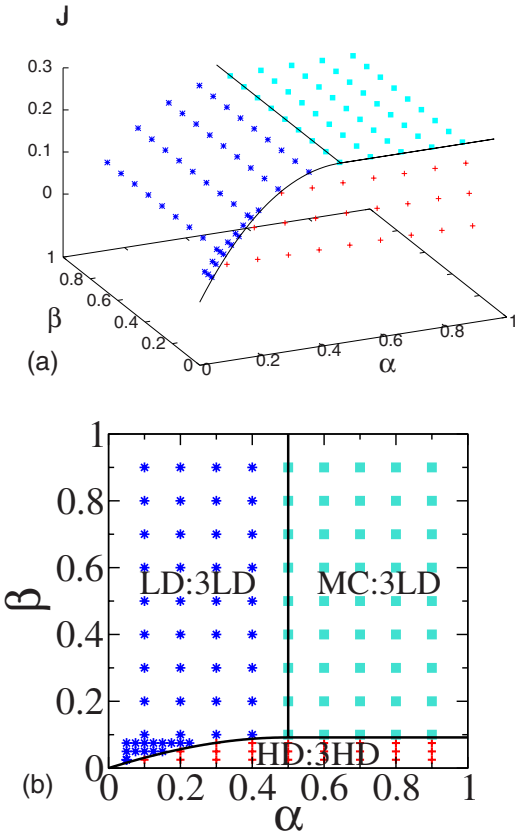

FIG. 11. (Color online) Current $J(\alpha,\beta)$ passing through a fourfold junction V(1:3). In (a), we plot the (simulation) total current J as a function of both α and β. In (b), we use a 2D projection to examine all cases of (α,β) and plot (as a minimum) a 10×10 grid of points (α,β), many more close to the curved phase boundaries. Symbols are attributed from simulations, where systems in phase LD:3LD are plotted as (blue) stars, MC:3LD as (turquoise) squares, and HD:3HD as (red) crosses. Based on the black lines, which represent theoretical mean-field phase transitions, the phase and current predictions in Eq. (17) can be judged accurate. This indicates that the analysis of Sec. III A correctly captures the phase behavior [cf. Fig. 10(a)].

in a 2LD:2LD phase, the current may be expressed as

$$2\times\alpha_A(1-\alpha_A)=J=2\times\alpha_B(1-\alpha_B), \tag{19}$$

where the rates are $\alpha_A=\alpha$ and $\alpha_B=\tilde{\rho}/2$. Substituting and solving for $\tilde{\rho}$ shows that the density $\tilde{\rho}$ at the junction is directly related to the overall input rate α as

$$\alpha=\tilde{\rho}/2 \tag{20}$$

(noting that $\alpha=1-\tilde{\rho}/2$ would contradict a LD phase for A, which excludes the second solution). The condition $\alpha<1/2$, which is necessary for a LD phase, must be respected, as well as $\alpha_A<\beta_A=1-\tilde{\rho}$. Putting both together shows that we are limited, in terms of $\tilde{\rho}$, to $\tilde{\rho}/2<1-\tilde{\rho}$, i.e., to $\tilde{\rho}<2/3$, that is $\alpha<1/3$—which therefore explains the critical value $\alpha^*=1/3$, at which we enter the saturated 2LD:2HD phase. This transition therefore pre-empts any occurrence of a MC phase. In essence, as the entrance rate α increases, the density at the junction must follow (twice as fast) to sustain the current out

of the junction, but since filling up the junction reduces the exit rate of segment A this ends up, at $\alpha^* = 1/3$, forcing segment A into a HD phase.

B. One in, three out—V(1:3)

In Sec. II above, we have described the approach as finding the intersections of functions of $\tilde{\rho}$ for the current through individual segments. This is indeed the most straightforward way of presenting the procedure and has furthermore allowed us to affirm the uniqueness of the solution, which we may now exploit. Technically speaking, however, splitting the parameter spaces of the individual TASEP segments along lines of fixed α and fixed β is not necessarily well suited to locating phase boundaries in the overall parameter space (α, β); whenever the boundaries do not follow these lines, as must be expected in general, we are then required to distinguish awkward subcases. In the following we will pursue the same strategy, but we adopt a slightly different angle, proceeding by enumeration of all candidate phases [53].

We use the example of the V(1:3) to rephrase the explicit-vertex framework to pursue this alternative but equivalent procedure. Again we start by defining the effective rates for each segment; these are simply

$$\beta_A = 1 - \tilde{\rho} \quad \text{and} \quad \alpha_{B_1} = \alpha_{B_2} = \alpha_{B_3} = \tfrac{1}{3}\tilde{\rho}. \tag{21}$$

Again this permits us to characterize the phase behavior of segment A and of the segments $B_{1,2,3}$ in terms of the effective rates, $(\alpha; 1-\tilde{\rho})$ and $(\frac{1}{3}\tilde{\rho}; \beta)$, respectively. As in Sec. III A above, the obvious fact that phases $B_{1,2,3}$ cannot be in a MC phase emerges correctly: the junction-site density, acting as an effective reservoir for several branches, cannot attain a high enough value α_B.

Rather than matching the currents through the individual segments directly, for all possible reservoir rates (α, β), we now consider all possible combinations of phases which might arise in the combined system—in this case, MC:3LD, MC:3HD, HD:3LD, HD:3HD, LD:3HD, and LD:3LD, i.e., all combinations of phases which do not involve a MC phase in the B segments. Any of these cases requires the effective rates on each individual segment to respect certain conditions, and imposing these simultaneously with the constraint of current conservation tells us for which conditions on the overall entrance/exit rates—if any—the corresponding case can arise in the combined system.

For an explicit example, consider the candidate phase combination MC:3LD. For segment A to be in phase MC, we must have (i) $\alpha \geq 1/2$ and (ii) $\tilde{\rho} < 1/2$, reasoning as before on mean-field results for individual segments (cf. Table I). For segments $B_{1,2,3}$ to be in phase LD, we must furthermore satisfy (iii) $\tilde{\rho} < 3\beta$. We now solve the matching condition on the currents,

$$J_{MC} = \frac{1}{4} = J_A = 3 \times J_B = 3 \times \frac{\tilde{\rho}}{3}\left(1 - \frac{\tilde{\rho}}{3}\right), \tag{22}$$

under constraints (i)–(iii). Doing so shows that the combined phase MC:3LD indeed arises, subject to the condition that the density at the junction takes on the particular value, $\tilde{\rho} = 3/2 - \sqrt{3/2}$, and that the exiting reservoir rate exceeds a lower limit, $\beta \geq \beta^* = \frac{1}{2} - \sqrt{1/6}$.

Analyzing all other combinations in a similar way, we obtain the combined mean-field phase diagram that is shown in Fig. 10(a). The corresponding current J can now be attributed trivially since the total current corresponds to the current flowing through segment A,

$$J(\alpha, \beta) = J_A = \begin{cases} \alpha(1-\alpha) & \text{(LD:3LD)}, \quad \text{i.e., } \beta > \beta^*(\alpha), \ \alpha < \frac{1}{2} \\ \frac{1}{2} & \text{(MC:3LD)}, \quad \text{i.e., } \beta > \beta^*(\alpha), \ \alpha > \frac{1}{2} \\ 3 \times \beta(1-\beta) & \text{(HD:3HD)}, \quad \text{i.e., } \beta < \beta^*(\alpha), \ 0 \leq \alpha \leq 1, \end{cases} \tag{23}$$

where $\beta^*(\alpha) = 1/2 - \sqrt{1/6}$ for $\alpha > 1/2$ and $\beta^*(\alpha) = 1/2 - \sqrt{1/4 - \alpha(1-\alpha)/3}$ for $\alpha < 1/2$. To verify Eq. (23), again we have run extensive Monte Carlo simulations, essentially as described in Sec. III A, but with particles on the junction choosing any of branches $B_{1,2,3}$ with equal probability 1/3. These numerical results again agree very well with mean-field predictions, as illustrated in Fig. 11, as well as the phase diagram in terms of the rate parameters α and β.

In terms of this phase behavior, several similarities but also qualitative differences arise with respect to V(2:2). First, the saturated phase once again involves a MC phase [something which does not occur for a V(2:2)], in the incoming segments, whereas the outgoing segments never exceed the LD state in this region. Second, the phase boundary between the entrance limited phase LD:3LD and the exit limited phase HD:3HD no longer coincides with the main diagonal, but it is now given by a parabolic profile of the form

$$\alpha(1-\alpha) = 3 \times \beta(1-\beta). \tag{24}$$

Both observations are related to the question of particle–hole symmetry, and we shall return to this point later (cf. Sec. III D). Finally, analyzing the above result for the current $J(\alpha, \beta)$ in parameter space reveals that the current is continuous across the phase boundary separating the low-density phase (LD:3LD) from the saturated phase (MC:3LD) and so is its first derivative. Consequently, the corresponding "transition" is seen to be of a *continuous* nature—again in contrast to the case V(2:2). Similarly, the values $\alpha, \beta = 1/3$ are no longer critical in this topology and do not give rise to any transitions.

C. Three in, one out—V(3:1)

The analysis of a fourfold junction V(3:1), which we shall call "reciprocal" with respect to V(1:3), goes through analogously to the analysis of the latter in Sec. III B above. The total current, which is now equivalent to the current passing through the exiting branch (B), is given by

$$J(\alpha,\beta)=J_{\mathrm{B}}=\begin{cases}3\times\alpha(1-\alpha) & (3\mathrm{LD}:\mathrm{LD}), \quad \text{i.e.,} \quad \alpha<\alpha^{*}(\beta), \quad 0\le\beta\le 1\\ \frac{1}{2} & (3\mathrm{HD}:\mathrm{MC}), \quad \text{i.e.,} \quad \alpha>\alpha^{*}(\beta), \quad \beta>\frac{1}{2}\\ \beta(1-\beta) & (3\mathrm{HD}:\mathrm{HD}), \quad \text{i.e.,} \quad \alpha>\alpha^{*}(\beta), \quad \beta<\frac{1}{2},\end{cases} \tag{25}$$

where $\alpha^{*}(\beta)=1/2-\sqrt{1/6}$ for $\beta>1/2$ and $\alpha^{*}(\beta)=1/2-\sqrt{1/4-\beta(1-\beta)/3}$ for $\beta<1/2$. As with V(1:3), we obtain a mean-field phase diagram [see Fig. 10(b)] and are able to compare theoretical predictions for currents and phase combinations to those obtained in Monte Carlo simulations; the results are entirely comparable to those for V(3:1) and therefore not shown here.

A maximum-current phase :MC is obtained, this time in the *outgoing* segment B, if both entrance and exit rates are sufficiently high, i.e., in the region where the overall current saturates. The maximum-current phase is complemented this time by a 3HD: phase in each incoming segment, in which particles accumulate before entering the junction. The phase boundary between the low-density (3LD:LD) and high-density (3HD:HD) phases is given this time by the parabolic relation,

$$3\times\alpha(1-\alpha)=\beta(1-\beta), \tag{26}$$

with a convexity which is opposite to the one in the case V(3:1). Inspecting the current $J(\alpha,\beta)$ shows that here it is the transition 3HD:HD vs 3HD:MC which is the (only) transition of a continuous nature. These results are again well corroborated by the corresponding simulation data.

D. Generalizing the particle–hole symmetry to reciprocal vertices

Linear TASEP is well known to obey a *particle–hole symmetry*, which may be stated in various fashions. It finds its simplest expression in the fact that the current achieved at a certain density $J(\rho)=\rho(1-\rho)$ is the same as that achieved at the complementary density $1-\rho$, i.e., $J(\rho)=J(1-\rho)$. This is rationalized by the microscopic argument that whenever a particle hops downstream, this may just as well be interpreted in terms of a hole hopping upstream, where the density of holes is of course $1-\rho$ and therefore the particle–hole symmetry is, at this level,

$$\rho\leftrightarrow 1-\rho, \tag{27}$$

$$J\leftrightarrow J. \tag{28}$$

We may also express this correspondence in terms of the rate parameters α,β and the resulting phase diagram. To this end consider the outlet of the segment where particles are extracted with rate β. The associated current of particles, traveling downstream out of the segment, is $\rho^{(\mathrm{OUT})}\beta$ in terms of the particle density ρ. This is of course equivalent to *injecting holes* at the same points, which will be successful with the probability of having the last site *empty of a hole*, i.e., occupied by a particle, such that $\beta\rho^{(\mathrm{OUT})}$ is also the current of *holes* traveling in the *opposite* direction. The full symmetry may therefore be written as

$$\alpha\leftrightarrow\beta, \tag{29}$$

$$\mathrm{HD}\leftrightarrow\mathrm{LD}, \tag{30}$$

$$\mathrm{MC}\leftrightarrow\mathrm{MC}, \tag{31}$$

$$x\leftrightarrow -x, \tag{32}$$

where the last line reminds us that we have also changed the direction along which the relevant entities are transported. We have implicitly used the convention that $x=0$ at the center of the segment and also the fact that a LD phase of particles (density ρ) is equivalent to an HD phase of holes (density $1-\rho$) and vice versa, whereas the MC phase may equivalently be described as a MC phase of holes or of particles.

In the presence of a junction, inspecting the phase diagrams for the reciprocal V(1:3) and for V(3:1) clearly suggests that they must be related through the same symmetry [see Figs. 10(a) and 10(b)], taking care of the additional change,

$$\mathrm{A}:\mathrm{B}\leftrightarrow\mathrm{B}:\mathrm{A}, \tag{33}$$

which is a straightforward consequence of the fact that holes travel in the opposite direction to particles and therefore experience the segments of the combined system in inverse order.

Nevertheless, this seemingly trivial generalization of the known particle–hole symmetry presents some subtleties on the microscopic level. To see this, consider the V(1:3). The only point requiring special thought is the junction point where the incoming segment branches into three outgoing segments. We reason first in terms of particles. The probability that a given attempt to move a particle leads to a displacement from the junction into whichever of the exiting branches is

$$\frac{1}{4L+1}\tilde{\rho}[1-\rho_{\mathrm{B}_{1,2,3}}^{(\mathrm{IN})}], \tag{34}$$

where we recall that L is the number of sites in each segment. The first two terms are the probabilities to select the junction site for a move and the probability to find it occupied by a particle. The third term is obtained as the total probability that this move succeeds, which may be thought of as the sum of three terms of the form $\frac{1}{3}(1-\rho_{\mathrm{B}_i})$ for $i=1,2,3$. Reasoning in terms of holes traveling upstream on the other hand, the equivalent process is to have a hole travel from whichever exiting branch into the junction. The density of holes being $1-\rho$, and $1-\tilde{\rho}$ at the junction, the probability for this to happen is

$$3\times\frac{1}{4L+1}[1-\rho_{\mathrm{B}_{1,2,3}}^{(\mathrm{IN})}][1-(1-\tilde{\rho}^{(\mathrm{IN})})], \tag{35}$$

which evaluates to *three times* the previous result.

The immediate conclusion is therefore that the microscopic particle–hole symmetry, as it is known from linear TASEP, may not be taken for granted at the junction point.

In terms of the resulting current, however, it must be observed that these microscopic events do not induce the same currents: whereas a particle hopping (downstream) from the junction into one of the B segments induces one unit of (particle) current *in the incoming branch*, one hole hopping (upstream) from one of the B segments into the junction induces one unit of (hole) current *in one of the outgoing branches*. The total contribution to the hole current, averaged over all three branches, is therefore one third, thus compensating the difference between the above probabilities for the microscopic events. Reasoning in terms of particles hopping downstream or in terms of holes moving upstream therefore indeed leads to identical currents, and we may affirm the resulting relation expressing the particle–hole symmetry for the transport characteristic,

$$J(\rho)=J(1-\rho), \tag{36}$$

despite the fact that we have seen that microscopic events do *not* respect particle–hole symmetry *at the junction site*. We shall illustrate further for a special case of V(2:2) in Sec. IV.

IV. PERIODIC-ON-AVERAGE CASE: FIGURE OF EIGHT

We now consider a special case of the above analysis, the *periodic-on-average* fourfold vertex, obtained by limiting the analysis of the vertex of type V(2:2) to the set of entrance/exit rates satisfying

$$\alpha=1-\beta. \tag{37}$$

This condition imposes periodic density profiles in the sense that the *average* density attributed to the exit reservoir $(1-\beta)$ is the same as that of the entrance reservoir (α). This may appear artificial, but it is in fact motivated by its link to a variety of related problems in different contexts:

(1) The periodicity of the density profiles means that we can build a square array of such pseudoperiodic V(2:2) vertices. In this sense, the periodic-on-average V(2:2) provides an even simpler regular planar lattice structure than the hexagonal lattice considered in [18].

(2) Equivalently, we may think of a chain of vertices, wherein successive vertices are connected by two parallel segments forming a braidlike structure of double segments periodically linked through a junction.

(3) We may think of a V(2:2) in feedback, with each exiting segment reconnecting to one of its entrance segments, thus producing two TASEP rings which share one site (the junction site). In terms of traffic models, this is equivalent to a crossing between two one-way lanes, at which each car takes a random decision as to which road to follow. It is therefore related to a special case in [23].

(4) Finally, the strictly periodic equivalent of this configuration is a figure of eight in which each particle crossing the junction decides at random which ring to follow. As such, we are dealing with a variant of the system proposed in [22] in an entirely different context.

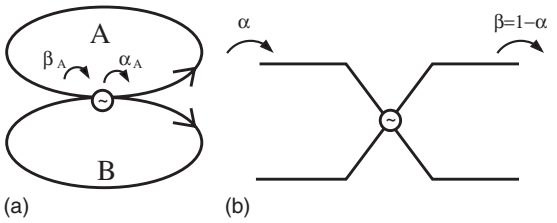

FIG. 12. (a) The figure of eight and corresponding effective rates at the junction. (b) Effective rates, corresponding to the bulk of the figure of eight, required for the corresponding periodic-on-average V(2:2).

Adopting the "figure of eight" as our vocabulary, we now discuss the overall current J as well as the density at the junction site $\tilde{\rho}$ in terms of a direct explicit-vertex analysis and make contact with the results for a periodic-on-average V(2:2). To do so, we will choose the overall density ρ (rather than the reservoir rate α) as control parameter, which allows for a more natural comparison between the open and the closed system variants and furthermore allows us to expose the physics in terms of the transport characteristic $J(\rho)$.

A. Effective rates

We denote the segments of the individual rings as A and B, respectively (see Fig. 12). From symmetry they must behave identically, their associated effective rates being set by the density at the junction site as

$$\alpha_{\mathrm{A,B}}=\alpha_{\mathrm{A}}=\alpha_{\mathrm{B}}=\tilde{\rho}/2 \quad \text{and} \quad \beta_{\mathrm{A,B}}=\beta_{\mathrm{A}}=\beta_{\mathrm{B}}=1-\tilde{\rho}. \tag{38}$$

From Table I we furthermore deduce that densities are given as

$$\rho_{\mathrm{A,B}}=\begin{cases}\alpha_{\mathrm{A,B}} & \text{if } \alpha_{\mathrm{A,B}}<\beta_{\mathrm{A,B}} \ \text{(LD)}\\ 1-\beta_{\mathrm{A,B}} & \text{if } \alpha_{\mathrm{A,B}}>\beta_{\mathrm{A,B}} \ \text{(HD)}.\end{cases} \tag{39}$$

From this the density at the junction can be directly deduced as follows.

B. Particle density at the junction

Neglecting finite-size effects due to the additional junction site we have $\rho \approx \rho_{A,B}$ for the overall density ρ. Substituting the effective rates [Eq. (38)] into Eq. (39) then shows that the overall density ρ is related to the density at the junction $\tilde{\rho}$ through

$$\rho = \begin{cases} \tilde{\rho}/2 & (\tilde{\rho} < 2/3) \ \text{(LD)} \\ \tilde{\rho} & (\tilde{\rho} > 2/3) \ \text{(HD)}. \end{cases} \tag{40}$$

This is consistent with the result we obtain from Eq. (18), arguing that the figure of eight is related to a periodic-on-average V(2:2) where the appropriate effective entrance/exit rates α and β for the V(2:2) are related to the *bulk* density of the figure-of-eight rings (see Fig. 12) through

$$\alpha = \rho_{A,B} \approx \rho \ \text{ and } \ \beta = \rho_{A,B} \approx 1 - \rho, \tag{41}$$

which indeed respects the condition of periodicity on average, $\alpha = 1 - \beta$. Substituting yields

$$\tilde{\rho} = \begin{cases} 2\rho & (\rho < 1/3) \\ 2/3 & (1/3 < \rho < 2/3) \\ \rho & (\rho > 2/3). \end{cases} \tag{42}$$

Figure 13(a) shows this relation, as well as results obtained from simulation. It immediately leads to several important conclusions. First, "slicing" through the phase diagram of a V(2:2) along the line $\alpha = 1 - \beta = \rho$ yields the correct behavior for a figure-of-eight system. Second, we must distinguish three different density regimes, and in particular there is a plateau for intermediate densities: on this plateau, even though the overall density in the system increases, the junction density remains constant. Third, the slopes of $\tilde{\rho}(\rho)$ are different for low and high densities, revealing that particles and holes behave differently, as suggested in Sec. III D. We shall return to this point shortly.

C. Transport characteristic curve

The associated current J flowing through the junction may be obtained from Eq. (17) by introducing the quasiperiodicity condition [Eq. (37)], i.e., essentially selecting the antidiagonal $\alpha = 1 - \beta$ of Fig. 9, as

$$J = \begin{cases} 2 \times \rho(1-\rho) & (\rho < 1/3) \\ 2 \times 2/9 & (1/3 < \rho < 2/3) \\ 2 \times \rho(1-\rho) & (\rho > 2/3). \end{cases} \tag{43}$$

This mean-field result is represented in Fig. 13(b) along with simulation data. The same regimes as for the junction density $\tilde{\rho}$ are apparent, and we now give a microscopic interpretation for all of them.

1. For low densities ($\rho < 1/3$)

We observe a classical TASEP transport parabola with doubled amplitude, i.e., $J = 2 \times \rho(1-\rho)$, as is easily justified. Both segments share only one site (the junction site) where an interaction might arise as particles compete for entering the junction. But since particle encounters are rare events at low densities, they cannot significantly affect transport in either segment, and so the total current is just twice a regular TASEP current.

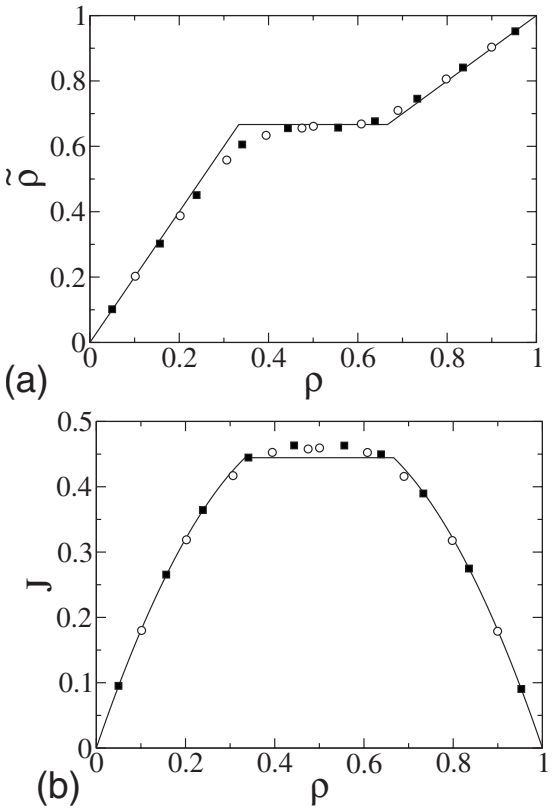

FIG. 13. Simulation data for a figure-of-eight network constructed both as a periodic-on-average vertex V(2:2) *and* as a proper closed system, respectively. Simulations use $L = 100$. Open symbols refer to open but periodic-on-average boundary conditions [i.e., V(2:2)]; closed symbols refer to closed boundary conditions (i.e., figure of eight). (a) shows the density at the junction site $\tilde{\rho}$ as a function of the overall density ρ; the flat line at $\tilde{\rho} = 2/3$ corresponds to the saturated-current plateau. The occurrence of two different slopes reveals the absence of particle–hole symmetry at the junction. (b) shows the total current J as a function of the overall density ρ; the plateau is $J_{\max} = 4/9$.

Remarkably, this hand-waving argument is extremely well respected up to a quite large density of $\rho = \frac{1}{3}$, as the simulation data show [see Fig. 13(b)], which seems to suggest that, in this regime, the mutual hindrance of particles at the junction has strictly no effect at all on the current. This appears counterintuitive but is in fact easily explained within mean-field theory by looking at the current entering the junction (the obvious bottleneck). We have

$$J = 2 \times \rho_{A,B}^{(\mathrm{OUT})}(1 - \tilde{\rho}), \tag{44}$$

where ρ_A is obtained (ρ_B is similar) injecting values from Table I, to obtain

$$\rho_A^{(\mathrm{OUT})} = \alpha_A(1 - \alpha_A)/\beta_A = \alpha(1-\alpha)/(1-\tilde{\rho}). \tag{45}$$

This shows that even though both $\rho_A^{(\mathrm{OUT})}$ and $(1-\tilde{\rho})$ vary with $\tilde{\rho}$, the current preserves its mean-field value, $2 \times \alpha(1-\alpha)$, through a compensation of two factors: while it

is true that adding particles to the junction must reduce the acceptance probability onto the junction and thus limit the current, we also see that the particle density in front of the junction builds up accordingly, thereby increasing the attempt frequency for moving particles onto the junction. In essence, whereas moving onto the junction becomes harder, more attempts are made, and the product of the two is constant, thereby maintaining the mean-field current as if there was no hindrance.

2. Transport plateau and phase coexistence ($1/3<\rho<2/3$)

As the overall density is increased beyond the critical value $\rho^*=1/3$, the density $\tilde{\rho}$ at the junction saturates at $\tilde{\rho}=2/3$. The occurrence of this plateau is reminiscent of phase coexistence. Further thought is required, however, in order to determine whether or not this translates into a plateau for the current characteristic $J(\rho)$.

We focus on discussing the case of a truly periodic (closed) system, where there is only one vertex, with density $\tilde{\rho}=2/3$ in the region of interest. For either segment the effective entrance rate is therefore $\alpha_{AB}=\tilde{\rho}/2=\frac{1}{3}$, and the effective exit rate is $\beta_{AB}=(1-\tilde{\rho})=1-2/3=1/3$. On the plateau we thus have $\alpha_{A,B}=\beta_{A,B}$, which is known to authorize LD/HD domain walls in the bulk of an individual segment, the position of which executes a random walk [34]. The plateau can therefore be interpreted as a coexistence between a high-density and a low-density zone which coexist within each *individual* ring and therefore involving a DW in each ring. The increase in overall density but at constant junction density $\tilde{\rho}^*=2/3$ may then be achieved through growth of the HD zones, at the expense of LD zones, which is furthermore compatible with the plateau in the associated current,

$$J_{\max}=2\times\tfrac{2}{3}\left(1-\tfrac{2}{3}\right)=\tfrac{4}{9}, \tag{46}$$

all throughout the region of intermediate densities ($\rho\in[1/3,2/3]$). This mechanism of a transport plateau due to phase coexistence is hence similar to what has been observed previously on a hexagonal structure [18,54].

The current-characteristic curve may therefore be interpreted as follows in terms of a successively growing overall density. After the parabolic increase discussed above, a plateau is reached via a discontinuous transition at an overall density of $\rho=1/3$. At this point a domain wall develops in both branches, thus allowing for the accommodation of coexisting LD/HD phases within both of the rings. As the overall density is increased further this does not lead to a further increase in the density at the junction nor in the current J: additional particles are accommodated simply through expansion of the HD zones (and corresponding displacement, on average, of the domain walls), while the associated mean-field current remains at its saturation value $J_{\max}=4/9$. Simulations show that this is qualitatively correct (see Fig. 13) but that the mean-field prediction *underestimates* traffic: the junction density saturates less quickly than expected as the critical value $\rho=1/3$ is approached; the current exceeds the mean-field prediction for the plateau, suggesting that some kind of collaborative motion may take over, exploiting constructively correlated fluctuations.

3. High densities ($\rho>2/3$)

The plateau finally ends at $\rho=2/3$, and standard TASEP transport resumes in both rings, without hindrance, making the transport characteristic $J(\rho)$ particle–hole invariant on the macroscopic level, as is to be discussed now.

D. Particle–hole symmetry and density at the junction

The initial slope $\tilde{\rho}\sim 2\rho$ for low densities is easily predicted by observing that the junction site is shared by two essentially independent TASEP segments: the random choice of particles leaving the junction furthermore explains that both rings are equally populated, and since particle collisions at the (shared) junction site are unlikely in the low-density regimes, the average junction density is therefore simply the sum of the average densities in each ring.

For high densities, we may attempt to reason in the same manner in terms of holes, but the argument must be modified. We may indeed expect twice as many holes to enter the junction site as would pass through any regular site in a linear TASEP segment (since the junction is fed through two segments). On the other hand, it is also true that they are twice as likely to exit the junction in the next step, as is best illustrated in an almost filled system: the hole effectively moves out of the junction whenever *either* of the particles in front of the junction is selected for a move, thus *doubling* the attempt frequency for hole displacements with respect to particle displacements at the junction site [such as in the comparison of Eqs. (34) and (35)]. This consequently and accordingly halves the particle's sojourn time on the junction site and, as a result, its average density.

In conclusion and as proposed in Sec. III D, the density at the junction density $\tilde{\rho}$ indeed reveals the absence of particle–hole symmetry on a microscopic level, in contrast to the transport characteristic $J(\rho)$, which respects particle–hole symmetry. Whereas the density at the junction site $\tilde{\rho}$ has initially been introduced as a somewhat formal coupling parameter, it is important to realize that it is a directly measurable quantity, and the example of a figure of eight shows that it indeed provides valuable insight into the system.

V. INTRODUCING RATE DISORDER AT JUNCTIONS: BIASED FIGURE OF EIGHT

We now generalize this analysis to the case where a *rate asymmetry* (cf. Sec. I) is present at the junction, i.e., where there is a bias for particles exiting the junction site to select one branch rather than the other (see Fig. 14 for an illustration). To do so, we shall first discuss a system consisting of two *parallel* segments, A and B, which share one site (the junctions) at each end. We first consider the (average) densities ρ_α,ρ_β on these junctions as externally constrained, which amounts to considering the junction sites to be coupled to reservoirs which maintain them at densities

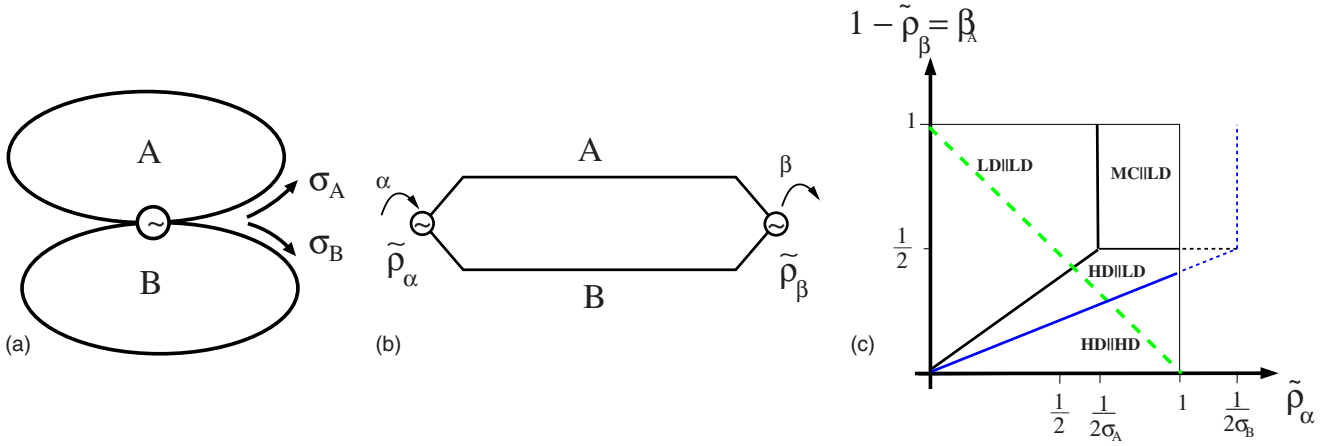

FIG. 14. (Color online) (a) Schematic representation of the figure of eight with a rate bias at the junction. A is the favored branch, which is selected with a probability $\sigma_A > 1/2$; branch B is selected with probability $\sigma_B = 1 - \sigma_A$. (b) Representation of the topology in terms of two parallel segments joined at junction sites, which are later to be matched. (c) The mean-field phases for a biased figure of eight are easily identified by considering the phases of two parallel sections A and B. For a general output rate β, two TASEP-like phase diagrams may be superposed in terms of the density at the junction $\tilde{\rho}$ after having expressed the input rates for the favored/unfavored branches A/B in terms of the associated bias σ_A (and σ_B). In particular, the bias favoring branch A ($\sigma_A > 1/2$) opens up a zone for the new HD‖LD phase, which widens as the bias becomes stronger. Note that the dashed parts of the phase diagram ($\alpha > 1/2$) are in fact inaccessible since the density at a junction cannot exceed unity. Since both branches are in parallel, no matching of currents is required at this stage. To conclude for a figure-of-eight topology, we must furthermore impose the condition of periodicity on average, $\beta = 1 - \tilde{\rho}$, which therefore limits the relevant phases to the first antidiagonal (dashed green line).

$\rho_\alpha = \alpha$ and $\rho_\beta = 1 - \beta$, respectively. We then require the average densities at the junctions to be identical, which essentially produces an open variant of the biased figure of eight. It will in fact be seen that this approach makes the rate asymmetry remarkably simple to handle within the explicit-vertex framework.

A. From two parallel segments to the biased figure of eight

We first determine the effective rates in this problem, denoting σ_A and σ_B the probabilities for a particle on the junction site to select branch A or B, respectively, such that $\sigma_A + \sigma_B = 1$. Without loss of generality we suppose $\sigma_A \geq \sigma_B$, i.e., branch A is favored by the bias. The effective rates are then

$$\alpha_A = \sigma_A \tilde{\rho}_\alpha, \quad \beta_A = 1 - \tilde{\rho}_\beta,$$

$$\alpha_B = \sigma_B \tilde{\rho}_\alpha, \quad \beta_B = 1 - \tilde{\rho}_\beta. \tag{47}$$

The exit rates are thus identical (i.e., $\beta \equiv \beta_A = \beta_B$) though the entrance rates differ due to the bias.

The phase behavior of each of the segments may now again be deduced from the standard TASEP phase diagram of a simple linear TASEP segment but with the input rates appropriately rescaled to accommodate the split and the bias at the "inlet" junction. Without bias both segments would give rise to the same phase behavior, which has been described for the symmetric figure of eight [cf. Sec. V, ultimately based on Fig. 6(b)]; in particular, the onset of the MC phase would be made irrelevant as its onset would be shifted to $\tilde{\rho} = \frac{1}{2\sigma} = 1$. The bias now lifts this degeneracy between the segments [cf. Fig. 14(a)], shifting the onset of the MC phase to $\tilde{\rho} = 1/2\sigma_A < 1$ in the favored branch A (thus making it accessible again) and to $\tilde{\rho} = 1/2\sigma_B > 1$ in the unfavored branch B (thus pushing it even further into the unphysical region). An illustration of the two superposed diagrams is shown in Fig. 14(c). Given that the two diagrams are represented in terms of $\tilde{\rho}_\alpha$, a variable which is relevant to both segments, all possible phase combinations for the two parallel phases (A‖B) may be simply read off: (LD‖LD), (HD‖LD), (MC‖LD), and (HD‖HD). Note in particular that the phase (HD‖LD) specifically depends on the presence of a bias ($\sigma_B < 1/2$): without bias this phase is collapsed onto the first diagonal, and it is unfolded due to the bias. A detailed discussion of all cases is presented in the Appendix.

At this stage the system under consideration consists of two segments linking two separate vertices, the densities ($\tilde{\rho}_\alpha = \alpha$ and $\tilde{\rho}_\beta = 1 - \beta$) of which are the control parameters. Rather than discussing the entire phase diagram system in detail, we immediately make contact with the biased figure of eight by imposing that both junctions must match and hence have identical densities,

$$\tilde{\rho} \equiv \tilde{\rho}_\alpha = \tilde{\rho}_\beta, \tag{48}$$

which is identical to reinjecting the condition of periodicity on average, $\alpha = 1 - \beta$. Only the antidiagonal $\tilde{\rho} + \beta = 1$ of the phase diagram in Fig. 14(c) is therefore accessible in the present case.

Following through with effective-rate (explicit-vertex) arguments, as for the previously discussed topologies, we can now determine the precise conditions under which either of the potential phases for the parallel (A‖B) segments may occur. This rather technical discussion is reproduced in the Appendix. In summary, the main results are the following. As the overall density increases, we can distinguish three successive regimes. For low overall densities, both rings are in a LD state. For intermediate densities, the ring favored by

the bias (A) switches into a HD phase, whereas the other one remains in an LD state. Finally, for high densities, both rings are in a HD state. We will discuss the properties of these phases before once again linking their transitions to the occurrence of domain walls.

B. Overall density and junction density

Regrouping the results for the overall density ρ in all individual cases [Appendix and Eqs. (A2), (A7), and (A12)], we can now invert them to express the density at the junction site as a function of the overall density, which varies from zero to unity,

$$\tilde{\rho}(\rho) = \begin{cases} 2\rho & (\mathrm{LD} \| \mathrm{LD}), \quad \rho < \frac{1}{2}\frac{1}{1+\sigma_A} \\ \frac{2\rho}{1+\sigma_B} & (\mathrm{HD} \| \mathrm{LD}), \quad \frac{1}{2}\frac{1+\sigma_B}{1+\sigma_A} < \rho < \frac{1}{2} \\ \rho & (\mathrm{HD} \| \mathrm{HD}), \quad \rho > \frac{1}{1+\sigma_B}. \end{cases} \tag{49}$$

This result is shown in Fig. 15 and compared to simulation results. The density at the junction follows the overall density in a piecewise-linear fashion, but several regimes arise for which different proportionality constants apply, in agreement with Eq. (42). These regimes are separated by zones for which no uniform mean-field solution is found and which we shall link to domain walls. Remarkably, the slope of the (linear) relationship between the junction density and the overall density is independent of the bias in the regimes of low density and high density, but it depends on it only in the intermediate phase (HD‖LD).

Observing the junction density $\tilde{\rho}$ therefore reveals that, in the presence of rate disorder on a figure of eight, there exist *two* plateau regions in the junction densities, i.e., two regions for which the density at the junction remains at a particular value despite an increasing overall density. Just as in the case of the unbiased figure of eight we attribute this to the occurrence of domain walls, such that two distinct phases coexist within a segment and such that the mean-field current saturates within this coexistence region.

C. Plateaus, phase coexistence, domain walls, and density gaps

For ease of reference, we state that, within mean-field theory, the two plateaus correspond to the density zones $G_{1,2}$, respectively, with

$$\rho \in G_1 = \left[\frac{1}{2}\frac{\sigma_A}{1+\sigma_A}, \frac{1}{2}\frac{1+\sigma_B}{1+\sigma_A}\right], \quad \rho \in G_2 = \left[\frac{1}{2}, \frac{1}{1+\sigma_B}\right]. \tag{50}$$

As in the nonbiased case, we associate the plateaus with coexisting phases within individual segments, but here the degeneracy is lifted by the bias. The first plateau corresponds to a HD-LD coexistence within the (favored) segment A since it corresponds to a value of $\tilde{\rho}_{G_2} = 1/(1+\sigma_A)$ of the junction density $\tilde{\rho}$. This translates into coinciding effective entrance/exit rates, $\alpha_A = \beta_A = \sigma_A/(1+\sigma_A)$, i.e., precisely to the condition for which phase coexistence arises on a linear TASEP segment. In the same manner, we link the second plateau ($\tilde{\rho}_2 = 1/(1+\sigma_B)$) to a LD-HD phase coexistence in branch B. From the simulation data for $J(\rho)$ presented in Fig. 15, the second plateau predicted from mean-field theory appears very clearly; the first one, rather narrow, is more difficult to pinpoint. We have verified the presence of such coexisting phases independently by directly detecting the associated domain walls in numerical simulations (see [18] for a description of a method for localizing such domain walls). As for the symmetric case, we defer a detailed discussion of DW dynamics to future work.

It may be helpful, as we proceed, to visualize how the density regions associated with these coexistence zones evolve as the bias is varied. Figure 17(a) presents the zones corresponding to on-segment coexistence for all values of the bias ($\sigma_A \geq 1/2$). This makes it apparent that both regions merge in the limit of vanishing bias ($\sigma_A, \sigma_B \to 1/2$), where we recover a single plateau with identical LD-HD phase coexistence ($\rho \in [\frac{1}{3}, \frac{2}{3}]$), thus correctly reproducing what appeared as a single transport plateau in the case of an unbiased figure of eight (cf. Fig. 13).

Conversely, we may conclude that the introduction of bias leads to a *splitting* of the single plateau at its center ($\rho = 0.5$), creating two separate regions of coexistence which evolve differently as the bias is increased.

D. Currents

We now turn to the current passing through each branch, which we can establish [from Appendix, for any overall density ρ and σ_A by simply adding Eqs. (A4), (A5), (A8), (A9), (A13), and (A14), respectively]

$$J_A(\rho) = \begin{cases} 2\sigma_A\rho(1-2\sigma_A\rho) & \mathrm{LD} \| \mathrm{LD}, \quad \text{i.e.,} \quad \rho < \frac{1}{2}\frac{1}{1+\sigma_A} \\ \frac{2\rho}{1+\sigma_B}\left(1-\frac{2\rho}{1+\sigma_B}\right) & \mathrm{HD} \| \mathrm{LD}, \quad \text{i.e.,} \quad \frac{1}{2}\frac{1+\sigma_A}{1+\sigma_B} < \rho < \frac{1}{2} \\ \rho(1-\rho) & \mathrm{HD} \| \mathrm{HD}, \quad \text{i.e.,} \quad \rho > \frac{1}{1+\sigma_B} \end{cases} \tag{51}$$

and

$$J_{\mathrm{B}}(\rho)=\begin{cases}2\sigma_{\mathrm{B}}\rho(1-2\sigma_{\mathrm{B}}\rho) & \mathrm{LD}\|\mathrm{LD},\quad \text{i.e.,}\quad \rho<\dfrac{1}{2}\dfrac{1}{1+\sigma_{\mathrm{A}}}\\ \dfrac{2\sigma_{\mathrm{B}}\rho}{1+\sigma_{\mathrm{B}}}\left(1-\dfrac{2\sigma_{\mathrm{B}}\rho}{1+\sigma_{\mathrm{B}}}\right)\dfrac{1+\sigma_{\mathrm{A}}}{1+\sigma_{\mathrm{B}}} & \mathrm{HD}\|\mathrm{LD},\quad \text{i.e.,}\quad \dfrac{1}{2}\dfrac{1+\sigma_{\mathrm{A}}}{1+\sigma_{\mathrm{B}}}<\rho<\dfrac{1}{2}\\ \rho(1-\rho) & \mathrm{HD}\|\mathrm{HD},\quad \text{i.e.,}\quad \rho>\dfrac{1}{1+\sigma_{\mathrm{B}}},\end{cases} \tag{52}$$

where we have also expressed the junction density in terms of the overall density [cf. Eq. (49)]. With some simplification, the resulting overall current $J=J_{\mathrm{A}}+J_{\mathrm{B}}$ can be written as

$$J(\rho)=\begin{cases}2\rho(1-2\rho+4\sigma_{\mathrm{A}}\sigma_{\mathrm{B}}\rho) & \mathrm{LD}\|\mathrm{LD},\quad \text{i.e.,}\quad \rho<\dfrac{1}{2}\dfrac{1}{1+\sigma_{\mathrm{A}}}\\ 2\rho\left(1-\dfrac{1+\sigma_{\mathrm{B}}^2}{1+\sigma_{\mathrm{B}}}2\rho\right) & \mathrm{HD}\|\mathrm{LD},\quad \text{i.e.,}\quad \dfrac{1}{2}\dfrac{1+\sigma_{\mathrm{A}}}{1+\sigma_{\mathrm{B}}}<\rho<\dfrac{1}{2}\\ 2\rho(1-\rho) & \mathrm{HD}\|\mathrm{HD},\quad \text{i.e.,}\quad \rho>\dfrac{1}{1+\sigma_{\mathrm{B}}}.\end{cases} \tag{53}$$

This shows immediately that, somewhat remarkably, the rate bias reveals the microscopic violation of particle–hole symmetry due to the topology at the junction and makes it observable even on the *macroscopic* level of the current-characteristic curve $J(\rho)$.

For two different biases, the density-dependent mean-field current J and the individual contributions $J_{\mathrm{A,B}}$ are plotted in Fig. 16. Many of the features of these curves may be rationalized by simple arguments. In particular, the current in zones of high and low overall densities rather closely follow the parabolae $J(\rho)\approx 2\times\rho(1-\rho)$, but the mechanisms are different for high and low densities.

We can now rationalize the overall $J(\rho)$ dependence through a succession of events as the overall density is increased.

1. Low densities: $\rho<1/2(1+\sigma_{\mathrm{A}})$

In the low-density limit, the individual currents very closely correspond to individual TASEP parabola of the form

$$\left.\begin{aligned}J_{\mathrm{A}}(\rho)&\approx 2\sigma_{\mathrm{A}}\rho(1-2\sigma_{\mathrm{A}}\rho)\\ J_{\mathrm{B}}(\rho)&\approx 2\sigma_{\mathrm{B}}\rho(1-2\sigma_{\mathrm{B}}\rho)\end{aligned}\right\}\quad \text{if}\quad \rho\ll 1, \tag{54}$$

which are also indicated in Fig. 16. This is indeed to be expected since, at low densities, each segment constitutes an effectively independent TASEP ring, with current $J_{\mathrm{A,B}}=\rho_{\mathrm{A,B}}(1-\rho_{\mathrm{A,B}})$. Since essentially all particle moves are accepted at low densities, the role of the bias at the junction is simply to distribute the $N=\rho 2L$ particles in a ratio of $N_{\mathrm{A}}/N_{\mathrm{B}}=\sigma_{\mathrm{A}}/\sigma_{\mathrm{B}}$ over the two segments (L being the number of lattice sites per segment). Thus, the resulting individual density of each segment (of length L) is

$$\rho_{\mathrm{A,B}}=\frac{N_{\mathrm{A,B}}}{L}=\frac{\sigma_{\mathrm{A,B}}N}{L}=2\sigma_{\mathrm{A,B}}\rho, \tag{55}$$

which leads to Eq. (54).

The agreement with simulation data, shown in Fig. 16, is excellent over a remarkably wide range of densities. Note also that, asymptotically for low densities, we have $J\sim 2\sigma_{\mathrm{A}}\rho+2\sigma_{\mathrm{B}}\rho=2\rho$, such that the initial slope of the overall current is indeed in agreement with the parabola given above (cf. Fig. 16).

For low densities, the state (LD‖LD) thus ensures a parabolic current characteristic, which has the initial slope of a (double) TASEP parabola, but then curves off *faster* than the latter, and the more so as the bias is stronger.

2. First coexistence zone G_1

In any case, the transport optimum corresponding to the summit of the parabola $[\rho^*=1/(1-4\sigma_{\mathrm{A}}\sigma_{\mathrm{B}})]$ is never reached but pre-empted by the first plateau, which corresponds to the point where the conditions of coexisting high- and low-density phases *within* the (favored) branch A are met. Direct observation from simulation confirms that this zone corresponds indeed to the presence of a domain wall in branch A.

3. Intermediate densities: $1/2(1+\sigma_{\mathrm{B}})/(1+\sigma_{\mathrm{A}})<\rho<1/2$

As the density is increased further, beyond the first plateau region, branch A is entirely filled up by a high-density phase: the domain wall disappears and we enter the regime where a high-density phase in the (favored) branch A is accompanied by a low-density phase in the (unfavored) branch B.

4. Second coexistence zone G_2

As soon as the overall density exceeds half-filling ($\rho>1/2$), we observe a second plateau region which corresponds to the complementary process observed earlier on: as the favored branch A cannot easily accept any further particles, these are now accommodated by the secondary branch B, in which we observe again a domain wall separating a

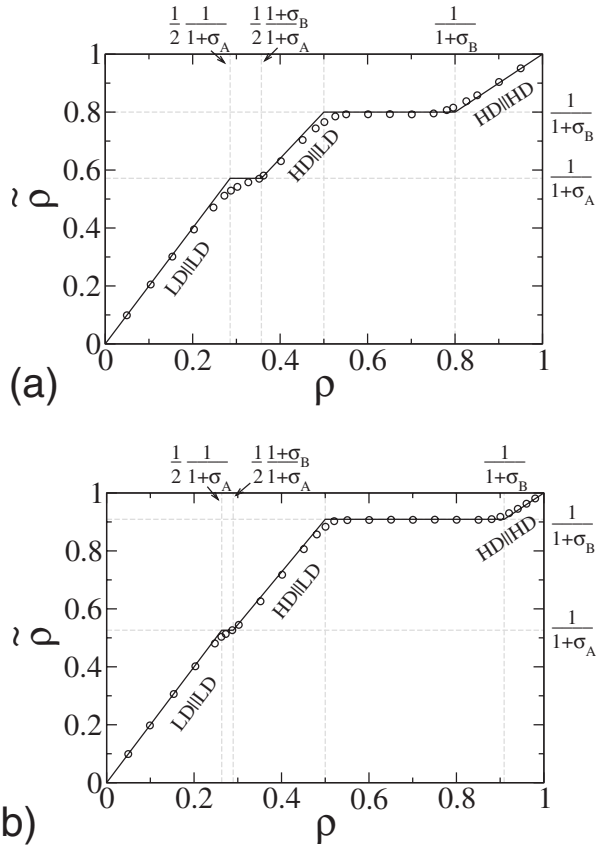

FIG. 15. Theoretical and Monte Carlo simulation (closed system) results for the junction density $\tilde{\rho}$: (a) an asymmetric split $\sigma_A=0.75$, $\sigma_B=0.25$; (b) $\sigma_A=0.90$, $\sigma_B=0.10$. Solid lines represent analytical predictions, gray grids indicate mean-field values for transition densities ρ and $\tilde{\rho}$. Theoretical predictions capture the behavior of $\tilde{\rho}$, although in simulations the transitions are not as sharp and fall below mean-field predictions, just as for the symmetric case [cf. Fig. 13(a)]. Note that the slopes in the (LD‖LD) and (HD‖HD) phases are *independent* of the exact junction asymmetry [cf. Eq. (49)], whereas the slope of the curve between the two plateaus depends on $\sigma_A=1-\sigma_B$.

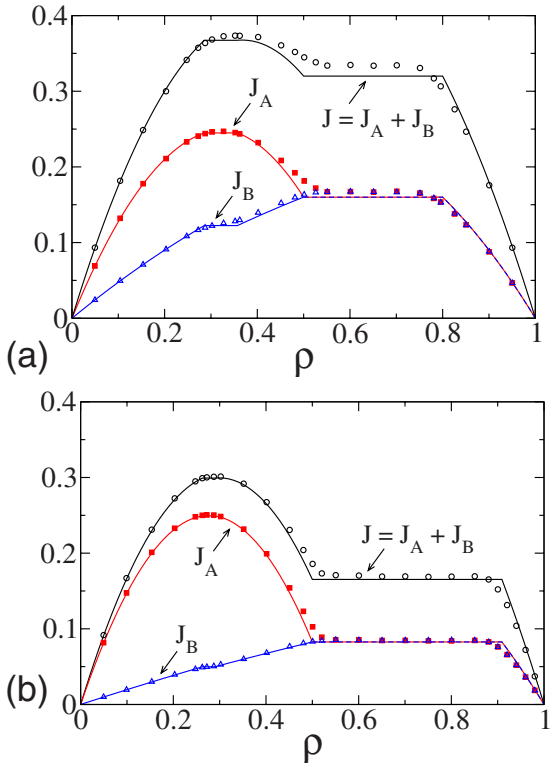

FIG. 16. (Color online) Theoretical and Monte Carlo simulation results for the currents J_A and J_B passing through individual branches and overall current J passing through a fourfold junction: (a) an asymmetric split $\sigma_A=0.75$, $\sigma_B=0.25$; (b) $\sigma_A=0.90$, $\sigma_B=0.10$. Solid lines represent theoretical predictions. As in the absence of bias ($\sigma_A=\sigma_B=1/2$, mean-field predictions for the current tend to underestimate the plateau current in a coexistence region [cf. Figs. 13(b) and 15].

low-density and a high-density region within this branch. From this point on, the mean-field currents carried by either branch are identical. The high-density region within the secondary branch B extends progressively as the overall density increases until it occupies the entire branch.

5. High densities: $\rho > 1/(1+\sigma_B)$

Once this critical density is exceeded, both branches now carry the same current, which we have already argued must be twice that of a standard TASEP parabola,

$$J(\rho) = 2 \times J_A(\rho) = 2 \times J_B(\rho) = 2 \times \rho(1-\rho) \quad \text{if} \quad 1-\rho \ll 1, \tag{56}$$

since the particle density is the *same* in both branches here: $\rho_A=\rho_B=\rho$. This concludes our discussion of the high-density limit.

This behavior of $J(\rho)$ is qualitatively confirmed by extensive numerical simulations (see Fig. 16), with two shortcomings. First, the current on the second plateau is underestimated by the mean-field approach, as was already the case for the symmetric figure of eight. Second, this underestimation extends also toward the zone prior to this plateau and particularly so if the bias is weak.

6. Optimal current

Crucial information on transport efficiency may now be obtained by determining the *maximum* current J_{max} which may be obtained for any given bias. To this end we point out that both plateaus correspond to saturated current (recall that the onset of the first plateau bridges the low-density transport parabola, as discussed above), and therefore the two candidates for optimal transport are the saturation currents of the plateaus, namely,

$$G_1: J_{G_1,\max} = \frac{\sigma_A(3-2\sigma_A)}{(1+\sigma_A)^2} \quad \text{and} \quad G_2: J_{G_2,\max} = 2\frac{1-\sigma_A}{(2-\sigma_A)^2}. \tag{57}$$

Note that both values tend to the (correct) saturation current of 4/9 for a symmetric figure of eight ($\sigma_A \to 1/2$). The first of these values is always higher for $\sigma_A \in [1/2, 1]$, suggesting that optimal transport is always achieved for rather *low* den-

sities, and particularly so if the bias is strong. Exceeding half-filling is detrimental whenever a bias is present.

The expression for the absolute maximum transport current (for a given bias σ_A) is hence established as

$$J_{\max}(\sigma_A) = \frac{\sigma_A(3-2\sigma_A)}{(1+\sigma_A)^2}, \tag{58}$$

where it must be remembered that we have assumed $\sigma_A > 1/2$ at the very beginning. The maximum of this function in the range $\sigma_A \in [1/2, 1]$ is therefore at $\sigma_A = 1/2$, confirming that the most efficient transport is achieved in the absence of bias, as was to be expected intuitively. The highest attainable current then drops from this optimal value of 4/9 toward the standard TASEP value of 1/4 as the bias increases toward total bias ($\sigma_A = 1$, $\sigma_B = 0$).

These results are presented in a complementary way in Fig. 17(b), where we superpose the complete transport curves $J(\rho)$ for various values for the bias σ_A. In addition to illustrating how the current is reduced as the bias increases, this representation helps us to establish the limiting cases. In the low-bias limit ($\sigma_A \to 1/2$) we recover the symmetric transport plateau with a saturation current of $J = 4/9$ associated with the V(2:2) and the equivalent figure of eight, as alluded to previously [cf. also Fig. 13(b)]. In the limit of total bias ($\sigma_A \to 1$), we recover a standard TASEP parabola with $J = 2\rho(1-2\rho)$, where the density enters *doubled* since particles from both rings are now exclusively located in the favored one.

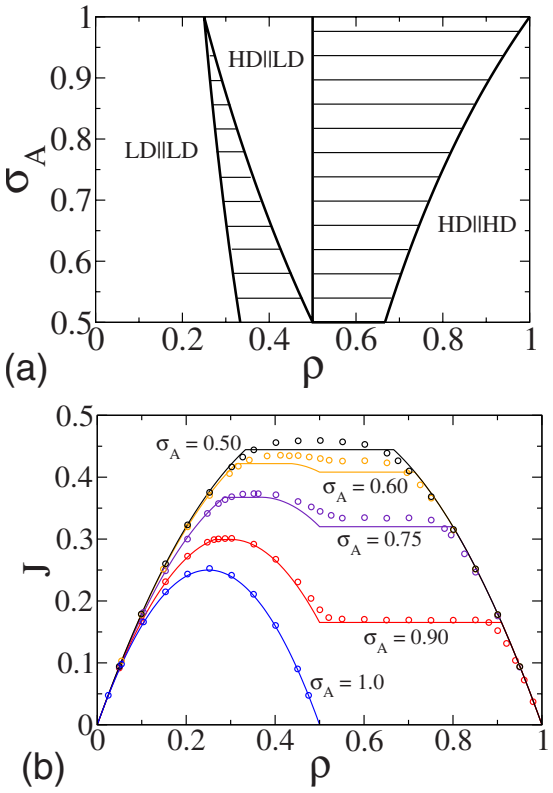

FIG. 17. (Color online) (a) Theoretical mean-field results illustrating the two coexistence regions (dashed) for the biased figure of eight as a function of the bias σ_A. The first zone corresponds to the presence of a domain wall in the favored branch A, whereas the second zone corresponds to a domain wall in branch B. For a given bias σ_A the current is constant within either of these domains (cf. Figs. 15 and 16). (b) Theoretical and Monte Carlo simulation results for the current J passing through a fourfold junction, with various values for the bias. Plotting several overall currents on the same graph allows us to demonstrate the limiting behavior of a biased figure of eight. In the limit $\sigma_A \to 0.5$, we recover the symmetric V(2:2) and the figure of eight [cf. Fig. 13(b)]. In the limit $\sigma_A \to 1$, we recover a standard TASEP parabola with $J = 2\rho(1-2\rho)$ (i.e., half of the sites become unusable). The underestimation of the overall current J tends to decrease as the system approaches more and more closely a standard linear TASEP: mean-field predictions work least well in the symmetric case.

VI. CONCLUSIONS

In this paper we have presented a mean-field framework, based on effective rates and explicit vertices, for analyzing TASEP-like transport on quasi-one-dimensional transport including branching. The approach consists of treating each segment as a TASEP segment, the behavior of which is governed by its entrance/exit rates. The topological coupling of segments is achieved by introducing an explicit *junction site* at which segments meet; the average particle density on the junction naturally parametrizes the effective entrance/exit rates at which particles enter/leave the individual segments adjacent to this junction. The phase behavior of the composed system may then be deduced by matching the well-known TASEP phases of the individual segments, subject to current conservation at the junctions. The density at the junction site, beyond being a convenient coupling parameter, in fact also constitutes a directly observable variable. We have shown that it captures fine details which are not necessarily reflected in the transport characteristic $J(\rho)$, and in particular shows the absence of particle–hole symmetry in a microscopic sense.

The proposed explicit-vertex procedure is robust and should in time permit the analysis of the stationary phases of TASEP-like transport through complex networks in a mean-field approximation; we furthermore expect it to generalize to transport models other than TASEP, provided only that the current of a segment $J(\alpha, \beta)$ is known in terms of its entrance/exit rates (as e.g., in [55]). In this paper we have applied it to TASEP transport through three variants of a fourfold vertex (one inlet and three outlets; two inlets and two outlets; and three inlets and one outlet), which constitute important elements for analyzing transport on a three-dimensional structure. We have constructed the phase diagrams of the composed system consisting of the junction and incoming/outgoing branches, in terms of global entrance/exit rates, as well as the associated currents, for all these cases. A detailed analysis of the periodic-on-average case, which for the symmetric fourfold vertex V(2:2) may be interpreted as a network with figure-of-eight topology on which two rings share the junction site, has shown the occurrence of domain walls, which lead to coexisting phases *within* a given segment. Although these require careful interpretation, their appearance is correctly detected based on the effective rates and the junction density. In the case of the figure-of-eight topology, we have furthermore shown that the associated

phase coexistence leads to a plateau in the current characteristic $J(\rho)$: such zones of *saturated current* generalize the notion of the maximal current phase on linear segments.

The case of the symmetric twofold vertex has furthermore allowed us to highlight that the notion of particle–hole symmetry is subtle in the presence of branching. Even where the transport characteristic $J(\rho)$ obeys the corresponding symmetry $J(\rho)=J(1-\rho)$, the average particle density $\tilde{\rho}$ measured locally at the junction site does not. Using effective rates to examine the microscopic processes at the branching point shows that the junction is indeed a somewhat particular site, at which the microscopic particle–hole symmetry does not apply. The junction density has been shown to reflect this, which again points to the junction density as a useful observable parameter, which may reveal such microscopic subtleties although they are not necessarily reflected in the global transport.

Finally, we have further generalized the explicit-vertex framework by considering transport on a *biased* figure of eight, in which particles leaving the (shared) junction site preferentially select one branch. We have established the resulting phase diagram, in which an additional phase arises which involves a saturated-current phase in the favored segment. In terms of the transport characteristic, we have shown two distinct plateaus to occur, which we link to coexisting phases and domain walls within one or the other of the branches. Remarkably, the bias entirely lifts the notion of particle–hole symmetry, such that even the transport characteristic $J(\rho)$ no longer obeys this symmetry, except for the limiting cases of total bias or vanishing bias.

In conclusion, we have built on the effective-rate approach [15] to construct an explicit-vertex framework, which is shown to be straightforward for analyzing mean-field transport on simple network structures involving branching. Applying it to further vertex types and extending it to handle complete networks are of course the next challenges but look achievable since the proposed procedures are entirely systematic. The smooth adaptation to the presence of a rate bias at a junction suggests that the approach may be sufficiently robust to handle even more complex situations, for example, the presence of other types of disorder. The issues of transport *dynamics* and of fluctuations, which have been shown to be rich even on simple regular structures [18], remain to be explored on more complex networks.

ACKNOWLEDGMENTS

We thank Paul Grassia for encouraging this collaboration. B.E. was supported by Grant No. MEST-CT-2004-503750 from the European Community.

APPENDIX: MEAN-FIELD PHASES IN THE BIASED-FIGURE-OF-EIGHT TOPOLOGY

We have shown in Sec. V that the phases of the two parallel segments forming a figure-of-eight system with a bias toward segment A are (LD‖LD), (HD‖LD), (MC‖LD), and (HD‖HD). In this Appendix we undertake a discussion in terms of effective rates as to conclude under which conditions these phases may arise. We also deduce the associated overall densities and currents.

1. Phase (LD‖LD)

For both phases $k=\mathrm{A},\mathrm{B}$, we must have (i) $\alpha_k \leq \beta_k$ and (ii) $\alpha_k \leq 1/2$. The former condition, which is more restrictive (and implies the latter), is expressed in terms of the junction density $\tilde{\rho}$ as

$$\tilde{\rho} \leq \frac{1}{1+\sigma_\mathrm{A}} \quad (\mathrm{LD}\,\|\,\mathrm{LD}). \tag{A1}$$

Since both segments have the same length and neglecting finite-size effects due to the additional junction site, we can deduce the overall density to be

$$\rho \approx \tfrac{1}{2}(\rho_\mathrm{A}+\rho_\mathrm{B}) \approx \tfrac{1}{2}(\alpha_\mathrm{A}+\alpha_\mathrm{B}) = \tfrac{1}{2}(\sigma_\mathrm{A}\tilde{\rho}+\sigma_\mathrm{B}\tilde{\rho}) = \tfrac{1}{2}(\sigma_\mathrm{A}+\sigma_\mathrm{B})\tilde{\rho} = \tfrac{1}{2}\tilde{\rho}, \tag{A2}$$

such that

$$\rho \approx \tfrac{1}{2}\tilde{\rho}. \tag{A3}$$

The associated currents are

$$J_\mathrm{A} = \alpha_\mathrm{A}(1-\alpha_\mathrm{A}) = \sigma_\mathrm{A}\tilde{\rho}(1-\sigma_\mathrm{A}\tilde{\rho}), \tag{A4}$$

$$J_\mathrm{B} = \alpha_\mathrm{B}(1-\alpha_\mathrm{B}) = \sigma_\mathrm{B}\tilde{\rho}(1-\sigma_\mathrm{B}\tilde{\rho}). \tag{A5}$$

Equations (A2)–(A5) fully characterize this phase.

2. Phase (HD‖LD)

We have the conditions (i) $\tilde{\rho} \leq 1/(1+\sigma_\mathrm{B})$ for segment B to be in a low-density phase (see above) as well as (ii) $\tilde{\rho} \geq 1/(1+\sigma_\mathrm{A})$ and (iii) $1-\tilde{\rho} \leq 1/2$, i.e., $\tilde{\rho} \geq 1/2$ for segment A to be in a high-density phase. The overall condition is therefore

$$\frac{1}{1+\sigma_\mathrm{A}} \leq \tilde{\rho} \leq \frac{1}{1+\sigma_\mathrm{B}} \quad (\mathrm{HD}\,\|\,\mathrm{LD}). \tag{A6}$$

The overall density is

$$\rho \approx \tfrac{1}{2}[(1-\beta_\mathrm{A})+\alpha_\mathrm{B}] = \tfrac{1}{2}(1+\sigma_\mathrm{B})\tilde{\rho}, \tag{A7}$$

and the associated currents are

$$J_\mathrm{A} = \beta_\mathrm{A}(1-\beta_\mathrm{A}) = (1-\tilde{\rho})\tilde{\rho}, \tag{A8}$$

$$J_\mathrm{B} = \alpha_\mathrm{B}(1-\alpha_\mathrm{B}) = \sigma_\mathrm{B}\tilde{\rho}(1-\sigma_\mathrm{B}\tilde{\rho}), \tag{A9}$$

thus fully characterizing this phase.

3. Phase (MC‖LD)

Here the conditions read (i) $\alpha_\mathrm{A} \geq 1/2$ and (ii) $\beta_\mathrm{A} \geq 1/2$ for segment A to be in a maximum-current phase, as well as (iii) $\tilde{\rho} \leq 1/(1+\sigma_\mathrm{B})$ for segment B to be in a low-density phase. These conditions may be written as

$$\frac{1}{2\sigma_\mathrm{A}} \leq \tilde{\rho} \leq \frac{1}{2} \quad (\mathrm{MC}\,\|\,\mathrm{LD}). \tag{A10}$$

These two inequalities are in fact mutually exclusive (since

$\sigma_A \leq 1$), *except* in the case of complete bias ($\sigma_A = 1$ and thus $\sigma_B = 0$), for which the figure of eight must reduce to a single TASEP segment. In Fig. 14, this case corresponds to the lower left corner of the (MC‖LD) phase touching the antidiagonal—but not for any other value $\sigma_A < 1$. Therefore, the (MC‖LD) phase cannot arise in the biased figure of eight (proper), and we do not discuss it further [56].

4. Phase (HD‖HD)

For both phases $k = A, B$, we must have (i) $\alpha_k \geq \beta_A$ and (ii) $\alpha_k \leq 1/2$; these are both satisfied if

$$\tilde{\rho} \geq \frac{1}{1+\sigma_B}. \tag{A11}$$

The overall density reads

$$\rho \approx \tfrac{1}{2}(1-\beta_A + 1-\beta_B) = \tilde{\rho} \tag{A12}$$

and the associated currents are

$$J_A = \beta_A(1-\beta_A) = (1-\tilde{\rho})\tilde{\rho}, \tag{A13}$$

$$J_B = \beta_B(1-\beta_B) = (1-\tilde{\rho})\tilde{\rho}. \tag{A14}$$

This concludes our discussion of the individual phase combinations. Implications for the overall behavior can be found in the main text (Sec. V).

[1] C. T. MacDonald, J. H. Gibbs, and A. C. Pipkin, Biopolymers **6**, 1 (1968).
[2] C. T. MacDonald and J. H. Gibbs, Biopolymers **7**, 707 (1969).
[3] Q.-H. Wei, C. Bechinger, and P. Leiderer, Science **287**, 625 (2000).
[4] A. Schadschneider, Physica A **285**, 101 (2000).
[5] C. Lutz, M. Kollmann, P. Leiderer, and C. Bechinger, J. Phys.: Condens. Matter **16**, S4075 (2004).
[6] A. Basu and D. Chowdhury, Am. J. Phys. **75**, 931 (2007).
[7] D. Helbing, Rev. Mod. Phys. **73**, 1067 (2001).
[8] V. Belitsky, N. Marić, and G. M. Schütz, J. Phys. A **40**, 11221 (2007).
[9] E. Frey, A. Parmeggiani, and T. Franosch, Genome Informatics **15**, 46 (2004).
[10] S. Klumpp, T. M. Nieuwenhuizen, and R. Lipowsky, Physica E (Amsterdam) **29**, 380 (2005).
[11] D. Chowdhury, A. Schadschneider, and K. Nishinari, Phys. Life. Rev. **2**, 318 (2005).
[12] A. Roux, G. Cappello, J. Cartaud, J. Prost, B. Goud, and P. Bassereau, Proc. Natl. Acad. Sci. U.S.A. **99**, 5394 (2002).
[13] G. Koster, M. VanDuijn, B. Hofs, and M. Dogterom, Proc. Natl. Acad. Sci. U.S.A. **100**, 15583 (2003).
[14] C. Leduc, O. Campas, K. B. Zeldovich, A. Roux, P. Jolimaitre, L. Bourel-Bonnet, and B. Goud, Proc. Natl. Acad. Sci. U.S.A. **101**, 17096 (2004).
[15] J. Brankov, N. Pesheva, and N. Bunzarova, Phys. Rev. E **69**, 066128 (2004).
[16] E. Pronina and A. B. Kolomeisky, J. Stat. Mech.: Theory Exp. **2005**, P07010.
[17] R. Wang, M. Liu, and R. Jiang, Phys. Rev. E **77**, 051108 (2008).
[18] B. Embley, A. Parmeggiani, and N. Kern, J. Phys.: Condens. Matter **20**, 295213 (2008).
[19] W. Thomson, Philos. Mag. **24**, 503 (1887).
[20] *The Kelvin Problem: Foam Structures of Minimal Surface Area*, edited by D. Weaire (Taylor & Francis, London, 1997).
[21] H. T. Lee, S. J. Neethling, and J. J. Cilliers, Colloids Surf., A **263**, 320 (2005).
[22] P. Pal, C. S. O'Hern, J. Blawzdziewicz, E. R. Dufresne, and R. Stinchcombe, Phys. Rev. E **78**, 011111 (2008).
[23] M. E. Foulaadvand and M. Neek-Amal, EPL **80**, 60002 (2007).
[24] S. A. Janowsky and J. L. Lebowitz, Phys. Rev. A **45**, 618 (1992).
[25] S. A. Janowsky and J. L. Lebowitz, J. Stat. Phys. **77**, 35 (1994).
[26] A. B. Kolomeisky, J. Phys. A **31**, 1153 (1998).
[27] J. Krug, Braz. J. Phys. **30**, 97 (2000).
[28] R. B. Stinchcombe, J. Phys.: Condens. Matter **14**, 1473 (2002).
[29] L. B. Shaw, A. B. Kolomeisky, and K. H. Lee, J. Phys. A **37**, 2105 (2004).
[30] P. Pierobon, M. Mobilia, R. Kouyos, and E. Frey, Phys. Rev. E **74**, 031906 (2006).
[31] P. Greulich and A. Schadschneider, J. Stat. Mech.: Theory Exp. **2008**, P04009.
[32] P. Greulich and A. Schadschneider, Physica A **387**, 1972 (2008).
[33] We use the term "mean field" throughout the paper, although there are various subtle points one should keep in mind that current and bulk density are proper mean-field quantities (for which, on the other hand, the mean-field expressions are known to be exact), but density profiles are *not*; in order to reconstruct density profiles one must invoke a domain wall theory on top of mean-field results, which retains collective fluctuations (shock fluctuations) in a phenomenological manner [34].
[34] A. B. Kolomeisky, G. M. Schütz, E. B. Kolomeisky, and J. P. Straley, J. Phys. A **31**, 6911 (1998).
[35] B. Derrida, E. Domany, and D. Mukamel, J. Stat. Phys. **69**, 667 (1992).
[36] G. Schütz and E. Domany, J. Stat. Phys. **72**, 277 (1993).
[37] B. Derrida, M. R. Evans, V. Hakim, and V. Pasquier, J. Phys. A **26**, 1493 (1993).
[38] B. Derrida, S. A. Janowsky, J. L. Lebowitz, and E. R. Speer, J. Stat. Phys. **73**, 813 (1993).
[39] K. Mallick, S. Mallick, and N. Rajewsky, J. Phys. A **32**, 8399 (1999).

[40] G. M. Schütz, *Phase Transitions and Critical Phenomena* (Academic Press, London, 2000), Vol. 19.
[41] B. Derrida, J. L. Lebowitz, and E. R. Speer, Phys. Rev. Lett. **89**, 030601 (2002).
[42] C. Enaud and B. Derrida, J. Stat. Phys. **114**, 537 (2004).
[43] B. Derrida, C. Enaud, and J. L. Lebowitz, J. Stat. Phys. **115**, 365 (2004).
[44] C. Boldrighini, G. Cosimi, S. Frigio, and M. Grasso Nuñes, J. Stat. Phys. **55**, 611 (1989).
[45] B. Derrida, J. L. Lebowitz, and E. R. Speer, J. Stat. Phys. **89**, 135 (1997).
[46] P. A. Ferrari and L. P. R. Pimentel, Ann. Probab. **33**, 1235 (2005).
[47] L. Santen and C. Appert, J. Stat. Phys. **106**, 187 (2002).
[48] *Nonequilibrium Statistical Mechanics in One Dimension*, edited by V. Privman (Cambridge University Press, Cambridge, 1997).
[49] G. M. Schütz, Diffus. Fundam. **2**, 5.1 (2005).
[50] P. Pierobon, A. Parmeggiani, F. von Oppen, and E. Frey, Phys. Rev. E **72**, 036123 (2005).
[51] J. Krug, Phys. Rev. Lett. **67**, 1882 (1991).
[52] J. S. Hager, J. Krug, V. Popkov, and G. M. Schütz, Phys. Rev. E **63**, 056110 (2001).
[53] This is formally closer to previous work [15–17] except that introducing the extra junction site makes our approach entirely systematic and that inaccessible subcases may be discarded very easily based on effective-rate arguments. Note also that our approach (as well as our results) furthermore differs significantly from those for a $V(1:m)$ with a synchronous update scheme [17].
[54] We do point out, however, that the analogous interpretation for a periodic-on-average but open system constructed from a V(2:2) requires further care: a full understanding of domain wall dynamics is required in this case, which cannot be achieved within the present framework since working with effective rates deduced from the average junction density necessarily neglects all correlation effects. For reasons of space and focus, we reserve this discussion for elsewhere.
[55] H. Hinsch and E. Frey, Phys. Rev. Lett. **97**, 095701 (2006).
[56] For completeness, however, we note that a (MC‖LD) phase *does* arise for a system consisting of two parallel sections, but it is effectively ruled out here through the condition of periodicity on average.